REVIEW ARTICLE

Check for updates

Plasma induced methane conversion: a review on CO$_x$-free production of hydrogen, valuable chemicals, and functional carbon materials

Xiaohan Chen,†^{ac} Bella, ID †^{ab} Yifei Yue,†^{a} Mohammadreza Kosari,^{abd} Lina Liu,^{e} Feiyang Hu,^{a} Keyu Cao,^{a} Yi Xiong,^{a} Aindrila Mandal,^{a} Jie Chang,^{b} Luwei Chen,^{b} Kang Hui Lim ID *^{a} and Sibudjing Kawi ID *^{a}

Catalytic decomposition and non-oxidative coupling of methane (CDM and NOCM) driven by plasma, especially non-thermal plasma, have been determined as strategic means for sustainable production of CO$_x$-free hydrogen and value-added chemicals. The 'one-step' direct CDM and NOCM bypass the need for intermediate syngas production to hydrogen and chemicals using the Fischer–Tropsch process, thus benefiting from energy savings, but nevertheless, are still plagued by poor yields and stability. Thermal, warm, and non-thermal plasma technologies have gained research momentum due to the efficacy for activation of strong C–H chemical bonds in methane. Herein, the current literature is firstly reviewed to elucidate the mechanistic insights and plasma synergies (with and without catalysts) for CO$_x$-free H$_2$ production *via* methane conversion with a particular focus on CDM and NOCM reactions. Our review ascertains that while plasma-assisted methane activation can resolve the need for high energy activation and dissociation of C–H bonds, the governing reaction pathways and difficulties in tuning product selectivity with plasma alone warrant further research on the role of plasma-catalysis as a promising solution to tune reaction selectivity. Additionally, we explore strategies for catalyst design and the selection of plasma sources to improve synergistic interactions in plasma-catalysis. Selected examples of catalyst use and reactor design in plasma-catalytic setups are presented. Finally, drawing from recent advancements and our research perspective, an advanced plasma integrated system is proposed, especially a concept for a plasma-catalytic reactor featuring a membrane separator, which may serve as an effective unit for hydrogen production and purification.

Broader context

The growing demand for sustainable hydrogen and carbon-neutral chemical production necessitates the development of CO$_x$-free methane conversion technologies. Plasma-driven catalytic decomposition (CDM) and non-oxidative coupling of methane (NOCM) have emerged as promising alternatives, bypassing syngas intermediates and enabling direct hydrogen and value-added chemical production. Non-thermal plasma (NTP) is particularly effective in activating methane's strong C–H bonds, yet challenges remain in enhancing reaction selectivity and stability. This review explores the synergy between plasma and catalysis, offering mechanistic insights and strategies for optimizing catalyst design and reactor configurations. A novel plasma-catalytic reactor concept with a membrane separator is proposed to improve hydrogen production and purification. By addressing current limitations and future directions, this review contributes to advancing plasma-assisted methane conversion toward a more sustainable energy landscape.

^{a} Department of Chemical and Biomolecular Engineering, National University of Singapore, Singapore 117585, Singapore. E-mail: E0030027@u.nus.edu, chekawis@nus.edu.sg

^{b} Institute of Sustainability for Chemicals, Energy and Environment (ISCE2), Agency for Science Technology and Research, Singapore 627833, Singapore

^{c} School of Chemistry and Chemical Engineering, Nanchang University, Nanchang, Jiangxi, 330031, China

^{d} Chemical and Biomolecular Engineering Department, College of Engineering, North Carolina State University, 911 Partners Way, Raleigh, North Carolina, USA

^{e} College of Environmental Science and Engineering, Ministry of Education Key Laboratory of Pollution Processes and Environmental Criteria, Nankai University, Tianjin 300350, China

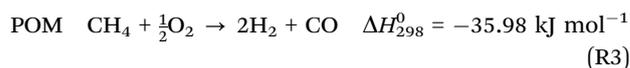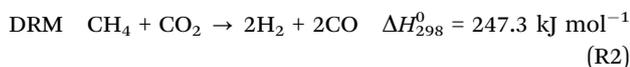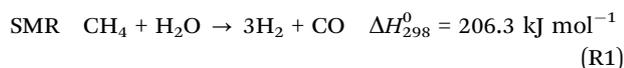† These authors contributed equally.

Introduction

The intensification of industrial processes has raised environmental awareness, driving demand for the development of sustainable and eco-friendly energy solutions.[1] The shift from fossil fuels to a carbon-neutral economy is necessary, with the term "hydrogen economy" coined by John Bockris in 1970, serving as a bridge solution.[2] Although hydrogen is widely regarded as a clean, CO$_x$-free energy carrier, its predominant

industrial production route—steam methane reforming (SMR)—remains highly energy-intensive, requiring approximately 206.3 kJ per mole of H_2 produced. Moreover, conventional SMR processes emit an estimated 9–12 kg of CO_2-equivalent per kg of H_2, depending on feedstock type, process efficiency, and carbon capture integration, thus contributing significantly to global greenhouse gas emissions.[3] Cleaner hydrogen production methods are crucial for addressing the growing energy demands of a hydrogen economy.

Methane, a major component of natural gas and a potent greenhouse gas, is notably emitted during crude oil extraction and has a stronger greenhouse effect than CO_2. Catalytic processes converting methane to CO_x-free hydrogen present a cleaner (i.e., 0.76–2.58 kg of CO_2-equivalent per kg of H_2),[4] low-cost alternative to fossil fuels. Due to its high hydrogen-to-carbon (H/C) ratio of 4 : 1, methane can theoretically yield up to 4 mol of H_2 per mole of CH_4, which is higher than ethane (3 mol H_2 per mol), propane (2.67 mol H_2 per mol), or butane (2.5 mol H_2 per mol), making it an attractive feedstock for hydrogen-rich processes.[5] Methane is a versatile feedstock commonly used to produce a wide range of specialty chemicals and fuels, including, but not limited to, hydrogen (e.g., via SMR, (R1)), syngas (via dry reforming of methane, DRM, (R2)), and methanol (via partial oxidation of methane, POM, (R3)).[6] However, the strong chemical bonds in methane (bond enthalpy of 413 kJ mol^{-1}) coupled with weakly polarized C–H bonds lead to a high barrier for methane activation and subsequent conversion to valuable products, necessitating thermal reactions at high temperatures (700–1100 °C), especially in the absence of a catalyst.[7] Hence, efficient catalytic technologies for methane conversion are essential to ensure sustainable processes and compete with conventional energy and commodity chemical production. Presently, methane is mainly utilized for hydrogen production via SMR, the most mature and dominant method of producing hydrogen on a large scale. However, despite its reliability and popularity, this process has a significant drawback of producing excessive amounts of CO_2 due to the reverse water gas shift (WGS, $CO + H_2 \rightarrow CO_2 + H_2$) reaction occurring as one of the side reactions. Another reforming reaction that is also growing in popularity is the dry reforming of methane (DRM); a reaction whereby CH_4 and CO_2 are reformed into syngas with an ideal H_2/CO molar ratio close to 1 (R2).[8–11] This reaction has garnered significant attention due to the possibility of using two greenhouse gases as feedstock, and the syngas produced can conveniently be integrated downstream to produce higher hydrocarbons via F–T synthesis.[12] In a similar context, the POM is another reaction producing a mixture of hydrogen and CO. This reaction produces a syngas H_2/CO ratio of 2 (R3), which is attractive for methanol synthesis.[12,13]

$$\text{SMR} \quad CH_4 + H_2O \rightarrow 3H_2 + CO \quad \Delta H^0_{298} = 206.3 \text{ kJ mol}^{-1} \tag{R1}$$

$$\text{DRM} \quad CH_4 + CO_2 \rightarrow 2H_2 + 2CO \quad \Delta H^0_{298} = 247.3 \text{ kJ mol}^{-1} \tag{R2}$$

$$\text{POM} \quad CH_4 + \tfrac{1}{2}O_2 \rightarrow 2H_2 + CO \quad \Delta H^0_{298} = -35.98 \text{ kJ mol}^{-1} \tag{R3}$$

In any case, different methane conversion routes must be considered when weighing in the CO_2 emissions involved and the desired products. In line with the hydrogen economy, two promising reactions are seen to be the potential answer: (1) catalytic decomposition of methane (CDM) and (2) non-oxidative coupling of methane (NOCM). CDM is a one-step endothermic reaction, traditionally performed to obtain carbon black for the tire industries. The process has been gaining attention in recent years due to its ability to readily produce CO_x-free hydrogen, which can be directly utilized in fuel cells.[14] Additionally, depending on the catalysts and reaction parameters, valuable carbon solids produced can be sold as other products, such as carbon black, nanofibers (CNFs), nanotubes (CNTs), nano-onions, etc. For instance, according to the literature, the most desired carbon product in CDM is CNTs, which, as of 2017 data, can cost up to $20 000 per kg.[15] Further details about CDM will be elaborated in the section "Catalytic decomposition of methane".

NOCM shares some similarities with CDM whereby hydrogen can be produced from the reaction without a reforming agent. However, instead of carbon solids, C_{2+} hydrocarbons are formed. Desirable products such as short-chain C_2 hydrocarbons (i.e., ethylene and acetylene), which are separated from hydrogen via polymeric membranes,[16] are important feedstocks in the chemical industry.[17] A summary of the current studies in catalytic NOCM is provided in the section "Non-oxidative coupling of methane".

Conventionally, CDM and NOCM have been catalyzed under thermal conditions, focusing on the selective production of value-added carbon products (e.g., olefins). However, such thermal processes require high reaction temperature (i.e., 500–800 °C for CDM, and 800–1100 °C for NOCM at ambient pressures) and heat supply due to their endothermic nature, making it challenging for process scale-up due to safety considerations. Plasma technology is of particular interest in resolving these challenges. Applying a plasma-induced electric field selectively increases the electron temperature in the reactant molecules, which renders it unnecessary for intensive heating to elevate the temperature in the bulk gas for the reaction to proceed over non-thermal and low-temperature plasma. Consequently, highly energetic electrons activate the reactant molecules via electron impact reactions to generate reactive plasma species (e.g., energetic electrons, radicals, and ions) that actively participate in the subsequent reaction pathways. While numerous research efforts have been directed towards more effective catalyst designs for methane conversion, novel ideas such as utilizing and integrating plasma into conventional thermocatalytic reactions are gaining attention due to the ability of plasma to activate thermodynamically stable gases with highly stable chemical structures such as methane,[18] carbon dioxide,[19] and nitrogen,[20] to facilitate their conversion into valuable products such as hydrogen, heavier hydrocarbons, and ammonia.[21,22] Compared with previous

reviews that primarily focus on plasma-assisted reforming,[39] this review uniquely highlights CO_x-free methane conversion (CDM and NOCM) routes using plasma, elaborates plasma–catalyst synergy and mechanistic insights, and proposes a novel membrane-integrated reactor design for simultaneous hydrogen production and separation. Therefore, in this review article, we mainly focus on combining plasma and catalysis in direct methane conversion to produce CO_x-free hydrogen and other value-added products, such as carbon solids *via* CDM and C_{2+} olefins *via* NOCM.

Plasma types and sources for chemical conversion

Research in plasma technology has been on a rapid rise in recent years, mainly because of its effectiveness in gas cleaning and conversion, chemicals production, and sterilization.[18,23,24] Plasma is an ionized gas consisting of ions, electrons, neutral compounds, radicals and excited species. As a 'fourth state of matter', plasma can be categorized into 'thermal plasma' and 'non-thermal plasma' depending on whether plasma itself is in thermal equilibrium or not. Plasma is said to be in thermal equilibrium when all of the species in the multicomponent system exhibit the same temperature in a localized area, and therefore, it is typically referred to as 'thermal plasma'. On the other hand, if there exist multiple temperatures within the plasma, the discharges are considered 'non-thermal plasma' as the species are not thermally equilibrated. Warm and cold plasma are also among other existing plasma types. The scope of this review will be limited to commonly applied plasma sources in plasma-catalysis, namely non-thermal and warm plasma.

Plasma can also be categorized based on its discharge modes, referring to (1) the method of plasma generation---such as dielectric barrier discharge, microwave, or radio-frequency systems—and (2) the nature of its interaction with the applied electric field, which governs electron acceleration, energy transfer, and discharge stability. The common discharge modes include: (1) dielectric barrier discharge (DBD): characterized by alternating current or pulsed voltage between two electrodes with a dielectric barrier to prevent arcing. DBD operates at atmospheric pressure and is widely used in surface treatment and gas-phase reactions due to its non-thermal nature;[25,26] (2) glow discharge: a low-pressure discharge where electrons collide with neutral gas molecules, causing excitation and ionization. This mode is commonly applied in thin-film deposition and material surface modifications;[27] (3) arc discharge: a high-current, low-voltage discharge that creates a highly ionized and thermal plasma. Arc discharge is suitable for high-temperature applications such as welding and carbon nanotube synthesis;[28] (4) microwave discharge: involves the generation of plasma using microwave radiation in the frequency range of 300 MHz to 10 GHz. It is electrode-less, reducing contamination and allowing applications in chemical vapor deposition and material synthesis;[29] (5) gliding arc
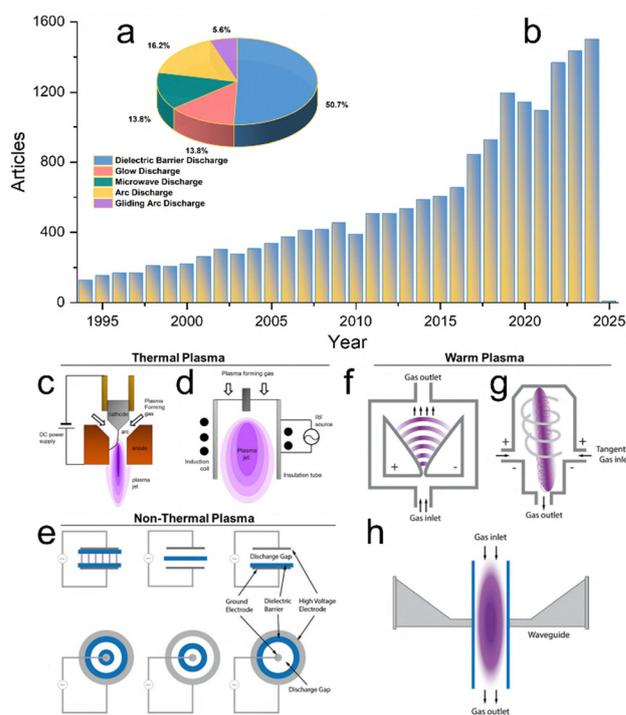

Fig. 1 Summary of recent plasma-catalysis literature: (a) the yearly number of articles published about plasma catalysis (17 922 in total for plasma and catalysis related articles), and (b) the percentage distribution of articles exploring various plasma discharge modes for plasma catalysis. Schematics designs of (c) and (d) thermal, (e) non-thermal (NTP), and (f)–(h) warm plasma sources. (c) Direct current (DC) plasma with non-transferred arc. (d) Radio-frequency (RF) plasma. Reproduced with permission from ref. 36 Copyright 2019 AIP Publishing. (e) DBD plasma with planar or cylindrical configurations. (f) Classical gliding arc (GA) plasma. (g) Gliding arc plasmatron (GAP) with reverse vortex flow GA. (h) Microwave (MW) discharge plasma. Reproduced with permission from ref. 24 Copyright 2017 The Royal Society of Chemistry.

discharge: combines features of thermal and non-thermal plasma, operating at atmospheric pressure. It is particularly useful for CO_2 conversion and syngas production.[30] The five discharge modes, among which the former one has received the majority of attention in recent years (Fig. 1a).

The classification of plasma into thermal and non-thermal categories, along with the discharge modes, highlights the diversity of plasma sources and their applications in plasma catalysis. Thermal plasma excels in high-temperature processes (typically above 5000 K), non-thermal plasma (NTP) is effective at low temperatures (with bulk gas temperature of 300–3000 K). Warm plasma, regarded as a subset of NTPs, operates in the intermediate range (1000–3000 K), bridging the gap between the two and offering a versatile approach for chemical conversions. The understanding of discharge modes further enhances the design and optimization of plasma systems for specific applications. Catalysts in the plasma discharge zone experience changes in electronic structure and surface properties, which can influence reaction intermediates and pathways. For plasma-assisted methane decomposition, recent DFT- and machine learning–augmented studies have shed light on how

CH_4 dissociation energy and carbon binding strength collectively determine reaction pathways. Wang et al.[31] constructed a comprehensive DFT database on single-atom alloys (SAAs) and demonstrated that metals such as Fe, Co, and Ni, while having favorable C–H dissociation barriers, differ in their atomic carbon adsorption energies—directly impacting whether filamentous carbon forms or pure H_2 evolves.[32] This insight guides the selection of carbon-tolerant catalyst systems for CDM under plasma environments. Hence, interest in plasma catalysis as a means to efficiently convert C1 molecules into various high-value-added chemicals and fuels has rapidly increased in recent years, as evidenced by a Web of Science search showing fast growth in articles published (Fig. 1b).

Thermal plasma

Thermal plasma, also known as hot plasma, can be achieved by several high-energy plasma sources (e.g., inductively-coupled plasma or ICP for short, plasma torch, arc plasma, etc.) where the ionized gases are in thermal equilibrium ranging from between 4000 K and 20 000 K.[24,33,34] High gas pressures can also result in thermal plasma as gas species would experience a smaller mean free path between collisions, thereby leading to more effective collisions (i.e., more efficient exchange of energy between electrons and gas particles). Specifically, higher pressures reduce the mean temperature differences in gas discharges and yield thermal equilibrium more efficiently.[35] One of the most common plasma sources is attained via a plasma torch, which can be operated by either direct current (DC) or radio-frequency (RF) (Fig. 1c and d).[36] A DC torch is made out of two electrodes (i.e., anode as a nozzle) powered by a high-voltage DC supply to generate an electric arc for gases to be heated up to 8000–16 000 K for a non-transferred DC torch design.[37] An RF plasma torch, on the other hand, consists of an induction (electromagnetic) coil and an insulation tube (Fig. 1d). An oscillating current in the induction coil produces an alternative magnetic field, which results in eddy currents producing heat via Joule heating.[36] The key advantage of the RF plasma torch is an electrode-less design that hence avoids degradation or corrosion. However, unlike the DC plasma torch, the maximum temperature obtainable is 10 000 K at a smaller plasma jet velocity.[36]

Non-thermal plasma

Warm plasmas are generally considered a subset of non-thermal plasmas, where a significant non-equilibrium exists between electron and bulk gas temperatures. However, unlike typical non-thermal plasmas such as DBD, RF, and glow discharges—with gas temperatures below 500 K—warm plasmas operate at significantly elevated gas temperatures, often exceeding 1000 K. Plasma sources such as gliding arc and microwave plasmas, though frequently labeled as non-thermal, can generate gas-phase temperatures well above 600 K and occasionally surpass 1000 K, placing them in an intermediate regime between conventional non-thermal plasmas and fully thermal plasmas like arcs and plasma torches.[38,39] These plasmas, which combine the advantages of both non-thermal and thermal plasma, have an average electron temperature of between 1 and 2 eV.[40] An example of a warm plasma source is gliding arc (GA) discharge, where the plasma is an auto-oscillating periodic discharge generated by two diverging electrodes (Fig. 1f). Given the poor interaction and contact with gas inflows in the classical design, a 3D cylindrical GA with vortex flow stabilization was developed (i.e., gliding arc plasmatron; GAP) (Fig. 1g).[41] Akin to RF plasma torch in thermal plasma, microwave (MW) plasma is also an electrode-less design version of warm plasma. MW plasma is powered by supplying electromagnetic radiation into a transparent discharge tube between 300 MHz to 10 GHz (Fig. 1h), and the resulting bulk temperature can reach up to 4000 K.[42,43] Non-thermal plasmas allow direct electron-induced dissociation of CH_4 (e.g., $e^- + CH_4 \rightarrow CH_3 + H + e^-$), circumventing the need for high bulk temperatures and enabling activation at $\sim$300–600 K.

Thermal vs. plasma catalysis in methane conversion: mechanistic differences

Methane conversion technologies are crucial for sustainable energy applications, particularly for achieving CO_x-free catalytic decomposition and non-oxidative coupling of CH_4.[44–46] Among various methods, thermal catalysis and plasma catalysis have gained attention due to their distinct mechanisms and complementary roles in activating CH_4,[47] and Table 1 highlights the key distinctions between these two routes, focusing on their roles in methane conversion. Thermal catalysis is a traditional approach where methane is activated through high temperatures, typically above 700 °C. The activation occurs via vibrational excitation and bond dissociation caused by heat, often in the presence of catalysts such as Ni, Pt, or Mo-based materials. The reaction pathways are governed by thermodynamic principles, where elevated temperatures provide the energy needed to

Table 1 Comparison between thermal and plasma catalysis

Aspect	Thermal catalysis	Plasma-catalysis
Energy source	External heat (e.g., furnaces)	Electric field, microwave discharge
Operating temperature	High ($>$700 °C)	Low (room temperature to $\sim$200 °C)
Activation mechanism	Thermal bond dissociation through vibrational excitation	Electron impact, ionization, and radical formation
Catalyst role	Lowers activation energy, enhances thermal stability	Provides active sites for plasma-generated species
Reaction pathways	Thermodynamically driven	Plasma-driven non-equilibrium pathways
Advantages	High reaction rates at elevated temperatures	CH_4 activation at low temperatures; reduced thermal stress
Disadvantages	High energy consumption; carbon deposition; catalyst sintering	Complex equipment, energy loss in plasma generation
Applications	Methane cracking, steam reforming	CO_x-free CH_4 decomposition, non-oxidative coupling

overcome the activation barrier. However, challenges such as catalyst sintering, carbon deposition, and high energy consumption limit its efficiency and scalability. Plasma-catalysis offering a new chemistry that is totally different than thermo-catalysis, on the other hand, leverages the synergy between non-thermal plasma and catalytic surfaces.[48] Non-thermal plasma generates reactive species, including radicals, ions, and excited molecules, through electron impact and electric field ionization. These species can directly activate CH_4 at relatively low bulk temperatures (room temperature to $\sim 200\,^{\circ}C$). Catalysts in plasma systems interact with these reactive intermediates, guiding the reaction pathways and improving selectivity towards desired products.[45]

Plasma-induced surface engineering strategies for enhanced catalyst performance

While the role of catalysts in modifying plasma chemistry has been discussed by many, it is clear that advanced surface engineering strategies are essential to improve catalyst stability, activity, and selectivity under plasma conditions. In both plasma-assisted NOCM and CDM, plasma-triggered restructuring of the metal–support interface (e.g., $NiO \rightarrow Ni^0$, $Ce^{4+} \rightarrow Ce^{3+}$) induces oxygen vacancies and highly active sites that promote CH_4 adsorption, CH_x stabilization, and C–C bond formation or C–H dissociation.

Defect engineering introduced via plasma irradiation—such as coordinatively unsaturated metal centers, edge sites, and oxygen vacancies—enhances CH_4 dissociation and intermediate coupling pathways, shifting selectivity toward light olefins in NOCM or facilitating clean hydrogen production in CDM.[49] Additionally, heteroatom doping (e.g., Na, K, La, N) modulates the electronic environment at active sites, aiding in intermediate stabilization, suppressing coke formation, and tuning reaction pathways.

Recent advancements in plasma-responsive catalyst architectures, such as "shielded bifunctional nanoreactors" (e.g., Na_2WO_4–Mn_3O_4/m-SiO_2), demonstrate up to 42% selectivity toward C_2 hydrocarbons under plasma activation, by spatially confining intermediate coupling and preventing deep dehydrogenation.[50] Likewise, Ni–γ-Al_2O_3 catalysts with noble gas co-feeding (Ar, He) exhibit improved energy efficiency and reduced coke formation, attributed to plasma–catalyst synergistic interface engineering.[49] Furthermore, plasma-assisted regeneration in CDM systems helps gasify soft carbon deposits and rebuild active sites, while strong metal–support interactions (e.g., Ni–CeO_2, Fe–ZrO_2) and confined metal clusters within porous matrices suppress sintering and maintain long-term stability.[51]

These advanced surface engineering strategies (Fig. 2)—encompassing interface reconstruction, defect creation, heteroatom doping, and structural confinement—constitute a comprehensive toolkit for optimizing catalyst performance under plasma conditions. They effectively align catalyst surface chemistry with
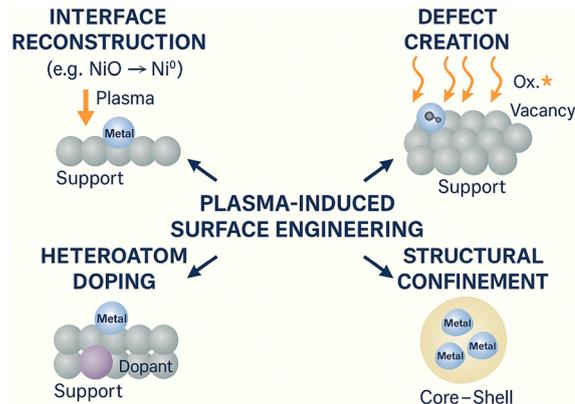

Fig. 2 Schematic illustration of plasma-induced surface engineering strategies for catalyst optimization under plasma conditions.

plasma-phase dynamics, enhancing olefin selectivity in NOCM, minimizing carbon deactivation in CDM, and ensuring durable operation in emerging plasma-assisted methane conversion technologies.

Mechanistic and design perspectives in plasma methane conversion

To further strengthen the understanding of plasma-catalytic mechanisms and promote rational catalyst design, recent studies have incorporated microkinetic modeling and density functional theory (DFT) simulations to explain observed experimental trends in plasma-assisted methane conversion. For example, Engelmann et al.[52] developed a plasma-specific microkinetic model that considers the influence of vibrationally excited CH_4 and plasma-generated radicals (e.g., CH_3^*, H^*) on methane coupling pathways over transition metals. Their results demonstrate that plasma conditions significantly shift the rate-determining step from CH_4 dissociation (dominant in thermal catalysis) to C–C coupling and product desorption, particularly on weakly binding metal surfaces such as Cu and Pd. These insights provide a theoretical basis for the experimentally observed enhancement in ethylene selectivity under non-equilibrium plasma environments.

Moreover, DFT calculations under electric field conditions have been used to examine CH_4 activation barriers and intermediate stability on metal and oxide surfaces. For NOCM, Maitre et al. developed a zero-dimensional nanokinetic model integrating plasma-phase radicals with surface microkinetics on a Ni(111) surface.[53] Their model demonstrates that plasma-generated CH_3^* radicals can promote surface CH_3^* coverage and enhance C–C coupling by stabilizing transition states and facilitating product desorption. Importantly, the model reveals that moderate CH_3^* coverage is optimal for maximizing C_2H_4 production, while excessive coverage can lead to deactivation or carbon buildup.

For plasma-assisted methane decomposition, recent DFT simulations have shown how electric fields and plasma species influence CH_4 dissociation and carbon nucleation pathways.

For example, external fields can reduce the activation barrier for C–H bond cleavage and stabilize surface-bound CH_x intermediates.[31] Additionally, the adsorption energy of atomic carbon on specific metal surfaces (e.g., Fe, Ni, Mo) determines the likelihood of filamentous carbon formation versus clean hydrogen evolution, offering guidance for selecting carbon-tolerant catalysts.

Building upon these mechanistic insights, recent literature has proposed a series of catalyst design strategies tailored for plasma catalysis, including: (i) heteroatom doping (e.g., Ga, Cu, Fe) to modulate surface electronic structure, enhance CH_4 activation, and stabilize CH_x intermediates, thereby promoting C–C bond formation and inhibiting coke deposition;[54] (ii) engineering strong metal–support interactions, such as Ni–CeO_2 and Fe–ZrO_2, to anchor active sites, enhance oxygen mobility, and reduce particle sintering and carbon accumulation;[55] (iii) defect engineering, including the creation of oxygen vacancies, to provide low-barrier activation sites for CH_4 and stabilize surface-bound CH_2^*/CH_3^* species under plasma excitation;[56] (iv) structural confinement strategies, such as core–shell catalysts and porous nanoreactors, to isolate active zones, limit radical over-reaction, and improve ethylene selectivity;[57] and (v) plasma-assisted surface reconstruction, where pre-treatment or in situ plasma exposure induces the formation of active facets, surface vacancies, or metal redistribution, leading to enhanced catalytic activity and carbon resistance.[58,59] These computational and experimental advances together establish a comprehensive approach to decipher reaction pathways and design next-generation catalysts for plasma-driven methane reforming, decomposition, and non-oxidative coupling reactions.

Methane conversion routes

The scope of this review is limited to "direct" methane conversion – wherein only methane reacts as the sole feedstock and no reforming agents are involved (e.g., CO_2 and H_2O), with the exception of processes whereby trace amounts of H_2O or CO_2 are present (possibly as byproducts) but not behaving as reforming agents. This definition has been used by other authors.[6,60,61] Direct conversion of methane, specifically CDM and NOCM, is of growing industrial significance as they are a means of CO_x-free hydrogen and high-value chemicals production, which is pertinent in the development of the hydrogen economy alongside other green hydrogen production methods, such as water electrolysis. Furthermore, processes involving hydrogen and chemicals (i.e., olefins, aromatics) production from methane are also particularly attractive as the industrial systems and infrastructures involved in the extraction, storage and distribution of methane-rich natural gas are already existing, extensive, and well-developed.[62–64] Unlike steam reforming which emits CO and CO_2, CDM/NOCM powered by plasma directly yield CO_x-free H_2 and valuable carbon/olefins, offering a cleaner pathway especially when powered by renewable electricity.

Currently, methane is converted into commodity chemicals via an "indirect" route, wherein methane is initially converted into syngas (i.e., CO and H_2) and by using appropriate catalysts, in which the syngas mixture is utilized in the subsequent production of a wide array of hydrocarbons or alcohols.[61,65] The indirect routes to syngas can be performed via different reactions such as reforming of methane, which includes steam (H_2O), dry (CO_2), partial oxidative (O_2), autothermal (O_2 + CO_2/H_2O), bi-(CO_2 + H_2O) and tri-(O_2 + CO_2 + H_2O) reforming, and coal or biomass gasification.[66–72] Further downstream processes to convert syngas—such as Fischer–Tropsch synthesis (typically operated at 200–350 °C and 2–5 MPa) or methanol and ammonia synthesis (200–300 °C and 400–500 °C, respectively)—are not only costly and energy-intensive due to their high-temperature requirements, but also face technical challenges such as heat integration complexity, separation and compression, cumulative energy loss across multiple steps, and reduced overall carbon efficiency, which complicate the production of desired chemicals (e.g., methanol, ammonia, etc.[73]) or synthetic fuels (e.g., diesel, jet fuel, etc.[74,75]). On the other hand, numerous research efforts have been directed towards "direct" methane conversion, in an attempt to produce high yields of desirable chemicals such as olefins, hydrogen or carbon solids. This approach aims to enhance the viability and competitiveness with the indirect route at higher cost effectiveness due to the void of separating unwanted by-products (e.g., H_2O) in "indirect" routes.[76,77]

Catalytic decomposition of methane (CDM)

For years, methane decomposition has been used to produce carbon black, predominantly via thermal plasma, which is useful for the rubber and tire industries.[78] Methane is decomposed into its components, which are hydrogen and carbon, according to the following reaction:[79,80]

$$CH_4 \rightarrow C(s) + 2H_2 \quad \Delta H_{298}^0 = 74.8 \text{ kJ mol}^{-1} \quad (R4)$$
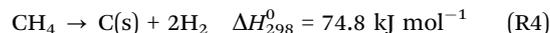
Depending on the catalysts and reaction parameters used, the morphology of the carbon solids can be tuned, ranging from carbon black to more valuable types such as CNTs,[81] which are highly desirable and profitable to be sold to offset the production costs. The CO_2 footprint of CDM is mainly derived from electricity generation (if renewable energy is not used) as well as during the extraction and transportation of natural gas. Compared to the industrial hydrogen production via SMR, whereby an additional water-gas shift (WGS) reaction must be carried out to increase the hydrogen yield, CDM is potentially advantageous as a 'one-step' process for H_2 production that does not require downstream H_2 purification from syngas. Additionally, CDM is often cited as more energy-efficient than water electrolysis, which requires 285.8 kJ per mole of H_2 produced. However, this advantage can be diminished by the fact that thermal CDM typically depends on high-temperature heat sourced from fossil fuel combustion, contributing indirectly to CO_2 emissions. In contrast, electrolysis can be powered by distributed renewable electricity, offering a cleaner alternative. Therefore, the true environmental and economic benefits of CDM depend heavily on the energy source used and the integration of carbon valorization strategies, such

as the selective production of high-value CNTs to offset operating costs.[14]

As the equilibrium conversion of CDM increases with temperature due to its endothermic nature, reaction kinetics are only reasonable at elevated temperatures above 1300 °C in the absence of a catalyst, which is not cost-effective. In this context, a stable and active catalyst becomes important, not only to reduce the energy barriers for the reaction but also to control the growth of carbon structures produced during methane decomposition. The carbon structures may either encapsulate the surface of the catalyst (which is commonly known as coking) or grow on top of the catalyst particle into filamentous carbon, commonly referred to as CNFs and/or CNTs. The latter is important as CNTs are extremely valuable in the microelectronics industry.

There are two important CNT growth mechanisms: base-growth and tip-growth. In the base-growth model, the carbon precipitates on the surface of the metal particle and subsequently crystallizes into a hemispherical dome. As the carbon precursor decomposes on the surface of the particle, with carbon diffusion moving upwards, the carbon filaments are formed on top of the metal particle (without the metal being detached from the support). Whereas according to the tip-growth model, carbon accumulates at the back of the metal particles, detaching it from the support and causing the metal particles to be embedded at the tip of the carbon filaments.[14] From a commercial perspective, it is more desirable to obtain base-grown CNTs due to the ease of CNT recovery (usually by means of fluidization) and catalyst regeneration. The metal nanoparticles would be more difficult to remove from tip-grown CNTs, whereby usually acid treatment would be required and thus shortening the length of CNTs produced. Additionally, it has been established that the chirality of CNTs also depends on the length and size of the nanotubes themselves, which ultimately will affect their performance and marketability for the production of materials,[82] such as transistors.[83] However, obtaining base-grown CNTs via CDM has been a challenge over the years, which makes it difficult to compete with the conventional chemical vapor deposition (CVD) method that is commonly used to fabricate base-grown CNTs.[84] Considering that the focus of the CVD process is solely on CNT production, CDM has the upper edge in being able to produce both CNTs and hydrogen in a high-throughput and sustainable fashion.

Nevertheless, there are several bottlenecks in the current state of thermally-driven CDM process that hinder its applicability for industrial hydrogen production: (1) high operating temperature due to its endothermic nature,[14] (2) severe catalyst deactivation due to coking and fast encapsulation of catalytic sites,[85] and (3) difficulty in controlling the desirable base-growth CNTs and carbon morphology.[86] Hence, increasing research attention has been devoted to the search for novel process technologies (e.g., plasma) to circumvent the abovementioned challenges.

Non-oxidative coupling of methane (NOCM)

The non-oxidative coupling of methane is a hydrogenation process that converts methane to short-chain C₂–C₄ hydrocarbons,
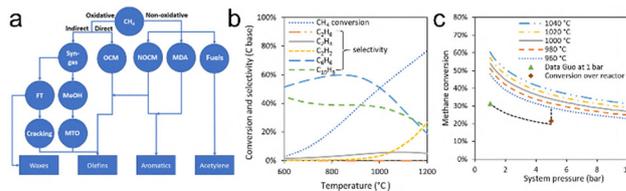

Fig. 3 (a) Converting methane to C_{2+} hydrocarbons via different conversion strategies, and (b) thermodynamic equilibrium methane conversion, C_{2+} product selectivity and (c) methane conversion at thermodynamic equilibrium as a function of reactor pressure for NOCM under thermal conditions are calculated using Aspen Plus[89] (MDA: methane dehydroaromatization). Reprinted with permission from ref. 17 Copyright 2021 American Chemical Society.

notably valuable olefins such as ethylene and acetylene, as well as aromatics such as benzene and naphthalene. As summarized in Fig. 3a, converting methane to C_{2+} hydrocarbons via different conversion strategies were reported. Besides, thermodynamic equilibrium methane conversion and C_{2+} product selectivity as a function of temperature, and methane conversion at thermodynamic equilibrium as a function of reactor pressure are calculated via Aspen Plus and shown in Fig. 3b and c.[17] Compared to oxidative coupling of methane (OCM) which produces byproducts such as H_2O and CO_2, NOCM offers an efficient route to directly produce H_2 without the need for downstream purification.[87] Industrial NOCM processes are conducted under intensive reaction conditions (> 1000 K), typically using an iron-based catalyst.[17] The list of reactions involved in NOCM is provided in Table 2.

Among these products, ethylene is of particular interest as it is a building block for major industrial reactions to manufacture valuable chemical products such as polymerization to polyethylene and oxidation to ethylene oxide.[88] Quite importantly, it is desirable in NOCM to limit the extent of side reactions (i.e., (R6) and (R7)) to maintain high purity of value-added C_2 products. However, a persistent bottleneck in thermal NOCM is that the formation of benzene and naphthalene is thermodynamically favorable at mild temperatures below 900 °C due to its lower enthalpy of reaction ((R7) and (R8)); hence the industrial NOCM process is highly energy-intensive as the reaction has to be conducted at temperatures above 900 °C in order to achieve good selectivity of C_2 products.[89] Recent technoeconomic analysis for designing thermocatalytic methane coupling processes showed that the cost of operating the reactor under severe reaction conditions comprises a significant cost of the overall process.[90] Rolf et al., conducted a comprehensive technoeconomic analysis of a simulated NOCM process with proposed reaction conditions of 1000 °C and 5 bar,[17]

Table 2 List of reactions involved in non-oxidative coupling of the methane process

Main product	Reaction		
Ethylene	$CH_4 \rightarrow 1/2C_2H_4 + H_2$	$\Delta H_{298}^0 = 101.1$ kJ mol⁻¹	(R5)
Acetylene	$CH_4 \rightarrow 1/2C_2H_2 + 3/2H_2$	$\Delta H_{298}^0 = 193.5$ kJ mol⁻¹	(R6)
Benzene	$CH_4 \rightarrow 1/6C_6H_6 + 3/2H_2$	$\Delta H_{298}^0 = 88.1$ kJ mol⁻¹	(R7)
Naphthalene	$CH_4 \rightarrow 1/10C_{10}H_8 + 8/5H_2$	$\Delta H_{298}^0 = 89.2$ kJ mol⁻¹	(R8)

showing that the resulting high heating duty for the methane feed (2.0 MJ $kg_{methane}^{-1}$) and reactor (1.7 MJ $kg_{methane}^{-1}$) remains a significant limitation of the current NOCM process design. In this regard, plasma is a promising technology that can overcome the energy barriers of NOCM, and consequently converts CH_4 to high value olefins without the incurrence of high heating supply. Due to the intense energy input required to achieve good C_{2+} olefin selectivity, plasma-catalytic systems have been seen as a possible innovation to overcome this limitation. We provide a detailed discussion of plasma-catalytic NOCM in the section "Plasma-assisted catalytic NOCM".

Roles of plasma-catalysis in CDM and NOCM

The use of plasma for methane decomposition is not a novel technique, and it can play an important role in both CDM and NOCM, as illustrated in Fig. 4, with considerable socio-economic potential. Plasma-assisted hydrocarbon decomposition dates back to the 1920s, initially aimed at carbon black production.[91] Later, methane was identified as a low-cost alternative to more expensive precursors like acetylene and ethylene, enabling co-production of hydrogen.[92] The discovery of single-walled carbon nanotubes (SWCNTs) by Iijima in 1991[28] sparked widespread interest in using methane as a carbon source for valuable CNT synthesis. Although other established methods such as chemical vapor deposition (CVD),[93] laser ablation,[94] arc discharge,[28] and electrolysis,[95] are tailored for CNT growth, these techniques primarily target carbon production and yield hydrogen only as a minor byproduct. In contrast, plasma-assisted CDM offers a pathway for the simultaneous high-yield co-production of both hydrogen and carbon nanomaterial. However, CDM processes especially at high throughput do not inherently offer precise control over CNT morphology, and may introduce challenges such as rapid catalyst deactivation, carbon encapsulation, and broad product distributions. Thus, while CDM has

economic promise, further innovation is needed to balance carbon structure control with process scalability.

The requirement for high energy to break the stable C–H bonds in methane, which is often achieved by high temperature, is a major concern from the aspects of safety and process economics.[24] As such, the introduction of an appropriate catalyst plays an important role in reducing the reaction temperature (i.e., by lowering the reaction barrier). However, as previously mentioned, several bottlenecks remain in thermally-driven CDM and NOCM processes, including high reaction temperatures, catalyst deactivation due to carbon encapsulation (particularly in CDM), difficulty in separating catalysts from solid carbon products, and poor control over the morphology and quality of carbon nanomaterials such as CNTs.[81,96]

Plasma has demonstrated its efficacy in lowering the barrier to methane activation through vibrational and electronic excitation of the reactants, thus circumventing the need for high-temperature reactions.[97,98] The production of reactive and energetic species, possibly vibrationally excited species in the gaseous phase, may come into contact with the catalyst surface. These vibrationally excited species can significantly enhance surface adsorption and desorption by lowering the activation barrier.[99] In addition to these gas-phase effects, plasma–catalyst interactions such as charge accumulation, surface polarization, and local electric field enhancement can also modulate the electronic structure and surface reactivity of catalysts, thereby influencing intermediate formation and catalytic selectivity.[100] Depending on the type and intensity of the plasma source (see section "Plasma Types and Sources for Chemical Conversion"), despite using methane as a sole feedstock, researchers have found ways to achieve different product selectivity from carbon black or solids, to desirable acetylene (C_2H_2) and ethylene (C_2H_4) and higher hydrocarbons (i.e., C_3 and above).[43,101–104] One will expect to generate mainly carbon solids from thermal plasma with methane, and coupled hydrocarbons even to C_6 if NTP is used.[105] In the following sections, we will focus our discussions on methane conversions to two product goals (i.e., carbon solids with hydrogen production or desired olefins/higher order hydrocarbons) using plasma and catalysts.

Plasma-assisted decomposition of methane

Conventionally, methane decomposition has been performed using thermal plasmas for hydrogen and carbon solids production. Specifically, plasma-driven pyrolysis of methane (as opposed to using thermal pyrolysis) has been developed and trialed for commercial production of carbon solids and hydrogen. Monolith Materials has recently operated a commercial-scale plasma pyrolysis plant, Olive Creek plant, in the United States at a technology readiness level of 8.[106] A thermal plasma (i.e., three-phase plasma torch) to give an average temperature of >2000 °C was the core technology for their efficient hydrogen production. In their lab-scale trials, $>99\%$ methane
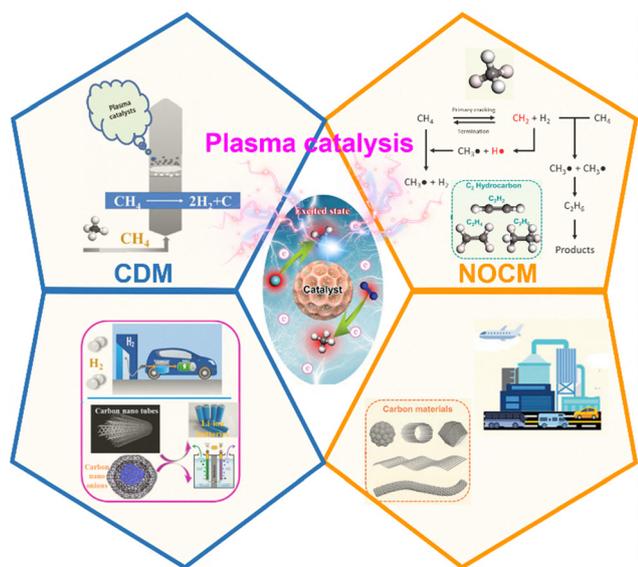

Fig. 4 Schematic diagram showing the role of plasma catalysis in CDM and NOCM and their socio-economic benefits.

conversion was achieved, with over 95% hydrogen selectivity and 90% hydrogen recovery. However, these performance metrics have not yet been fully replicated at the commercial scale. In pilot-scale thermal plasma systems, hydrogen production required only $\sim$25 kWh per kg H_2—approximately 40% of the energy needed for water electrolysis ($\sim$60 kWh per kg H_2)—but challenges such as reactor stability, carbon deposition management, and electrode degradation were encountered, indicating the need for further optimization before large-scale deployment. Moreover, plasma-assisted decomposition of methane coupled with renewable electricity has significantly lower CO_2 emissions than competing H_2-producing technologies (*i.e.*, steam methane reforming and thermal pyrolysis of methane).[107] Hence, there is great potential in implementing plasma to assist with methane decomposition reactions.

Mechanistic insights of CDM

Thermal methane decomposition has been studied quite extensively from both experimental and theoretical points of view, although it remains a controversial topic. Traditionally, this reaction was performed without any catalyst. Since the 1960s, various reaction mechanisms have been proposed under similar operating conditions. One of the earliest studies was conducted by Skinner and Ruehrwein, using shock-tube experiments to measure the initial rate of methane dissociation.[108] Since then, researchers have found that uncatalyzed methane decomposition involves free-radical formation, where the initiation step corresponds to the dissociation of methane into a methyl radical and a hydrogen atom.[14] A detailed reaction mechanism for the uncatalyzed methane decomposition was proposed by Chen *et al.* in 1976,[109] which is summarized in Fig. 5.[14] Their mechanism was built on the basis of C–H bond cleavage and the subsequent methyl radicals formation.

An alternative reaction mechanism has also been postulated by Kevorkian *et al.*[110] and Kozlov and Knorre,[111] whereby the
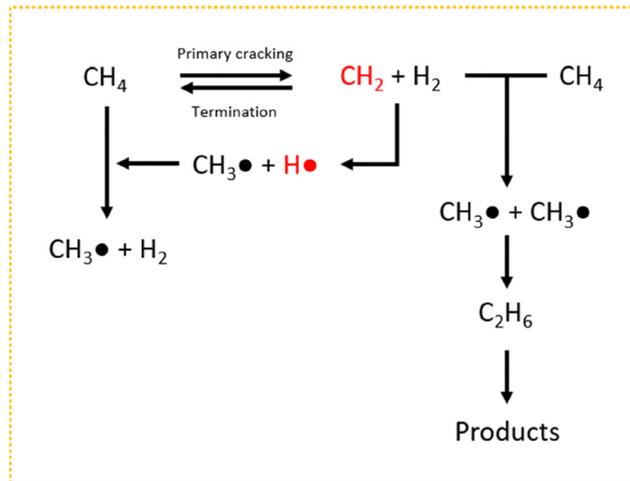
Fig. 6 Non-catalytic methane decomposition reaction mechanism where primary rupture to CH_2 and H_2 is the rate-determining step.[110,111]

rate-determining step is the dissociation of methane to form methylene (instead of methyl radical) and a hydrogen molecule (instead of a hydrogen atom), as shown in Fig. 6. The controversial results may be due to the different temperature conditions used by different authors. For instance, it has been shown that the dissociation of methane into a hydrogen atom and a methyl radical is typically encountered in experiments carried out at low temperatures (*i.e.*, <1400 °C). Whereas the decomposition into hydrogen molecule and methylene has been observed in reactions carried out at higher temperatures (*i.e.*, >1400 °C).[112]

In contrast, plasma-assisted CDM presents different mechanistic behavior. Optical emission spectroscopy (OES) and laser-induced fluorescence (LIF) can detect CH_3^*, CH_3^*, and H^* in the gas phase, while *in situ* DRIFTS or mass spectrometry reveal surface-bound intermediates. Electron impact dissociation dominates radical generation, which can proceed toward full methane decomposition or couple into C_{2+} species (relevant to NOCM).

To address the discrepancies in proposed mechanisms—namely, methane decomposition *via* methyl radicals ($CH_3^* + H^*$) *versus* methylene intermediates ($CH_2^* + H_2$)—future efforts should focus on integrating advanced spectroscopic and computational methods. For example, *in situ* OES and LIF can help identify key plasma-phase radicals (CH_3^*, CH_2^*) under varying energy input and temperature regimes. Similarly, *in situ* DRIFTS or mass spectrometry (MS) could reveal adsorbed CH_x^* species on catalyst surfaces, providing direct mechanistic evidence. On the computational front, density functional theory (DFT) and *ab initio* molecular dynamics (AIMD) simulations under both thermal and electric field-assisted conditions may elucidate the energy profiles and rate-determining steps of competing pathways. By correlating experimental signatures with theoretical insights, the dominant decomposition mechanism, whether methyl radical or methylene-driven, can be systematically identified under specific plasma-catalytic conditions.
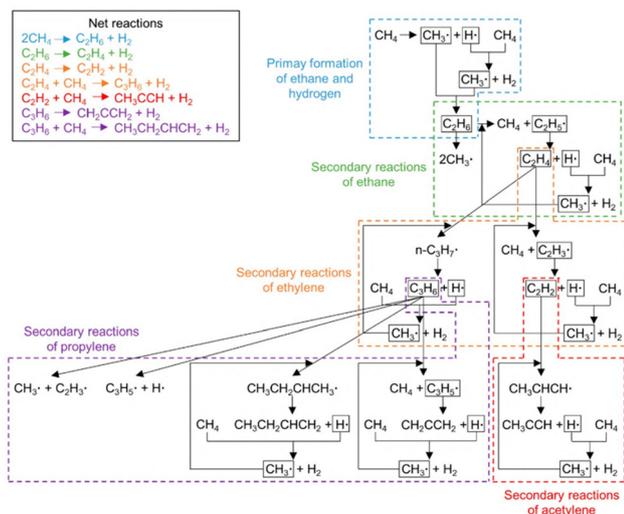

Fig. 5 The reaction mechanism of uncatalyzed methane decomposition as proposed by Chen *et al.*[109] Reproduced with permission from ref. 14 Copyright 2021 American Chemical Society.

Methane decomposition has been carried out using thermal plasma reactors, however, they are often operated without the presence of catalysts because thermal plasma is suitable for endothermic reactions such as CDM, as the reactors are typically operated at temperatures $>1000\,°C$.[113] In plasma-assisted methane conversion, it has been widely accepted that different operating conditions and plasma sources and/or forms will result in different methane conversion rates and selectivity towards certain products.[114] One of the pioneering studies in understanding the reaction mechanisms in thermal plasma methane decomposition for carbon solid production was performed by Fincke *et al.*, where the experimental work was carried out using a modified thermal DC plasma reactor in the absence of a catalyst.[92] Specifically, they modified the plasma reactor to increase the residence time of the reactant in plasma, which resulted in an increased selectivity from acetylene to carbon solids to give a 6-fold increase in yield. The authors proposed that there exists a kinetically-limited process through acetylene decomposition (*via* benzene) during the soot formation.[92] A more recent study was performed by Gautier *et al.*, where they conducted computational studies to understand the phenomenon occurring inside an AC-powered 3-phase thermal plasma process prototype that has been developed for over 20 years at MINES-ParisTech.[115] Through numerical modeling and CFD studies, they attempted to develop a deeper understanding of the processes happening during the nucleation and growth of carbon (black) particles. The studies of Gautier *et al.* were partially based on Fincke *et al.*'s findings, where the carbon precursors are observed to form from acetylene and benzene.[115]

In general, thermal plasma gives rise to very high ionization rates in the gaseous phase to induce Joule heating. And in doing so, the high bulk temperature can rupture the stable C–H bonds in methane. As highlighted by previous studies, the formation of carbon solids (*i.e.*, carbon black) or soot is from acetylene as a carbon precursor. We note the distinction between carbon black and soot is produced depending on whether the carbon solids formation is intended under controlled conditions (*i.e.*, carbon black) or uncontrolled undesirable formation (*i.e.*, soot).[116] In the presence of thermal plasma, high concentrations of acetylene were produced, which would react with one another to form aromatic compounds (*i.e.*, polycyclic aromatic hydrocarbons (PAHs)) through a H-abstraction-acetylene-addition (HACA) mechanism.[117,118] Nucleation begins with collisions of PAHs to produce nuclei of 10–20 aromatic rings, and further coalescence results in a viscous tar. The nano-droplets then undergo rearrangement, further nucleation at the surface, and loss of hydrogen until a solid (*i.e.*, carbon black) is formed.[116] Kreuznacht *et al.* studied the use of microwave plasma torch (*i.e.*, warm plasma) and GAP (*i.e.*, gliding arc plasmatron; warm plasma) in methane decomposition.[43] It was found that methane conversion was twice as high in GAP configuration than in the plasma torch at the same specific energy input and methane feed concentration (Fig. 7a and c), attributed to a larger reaction volume in the rotational vortex flow (Fig. 7e). Also, a higher concentration of CH_4 would lead to higher
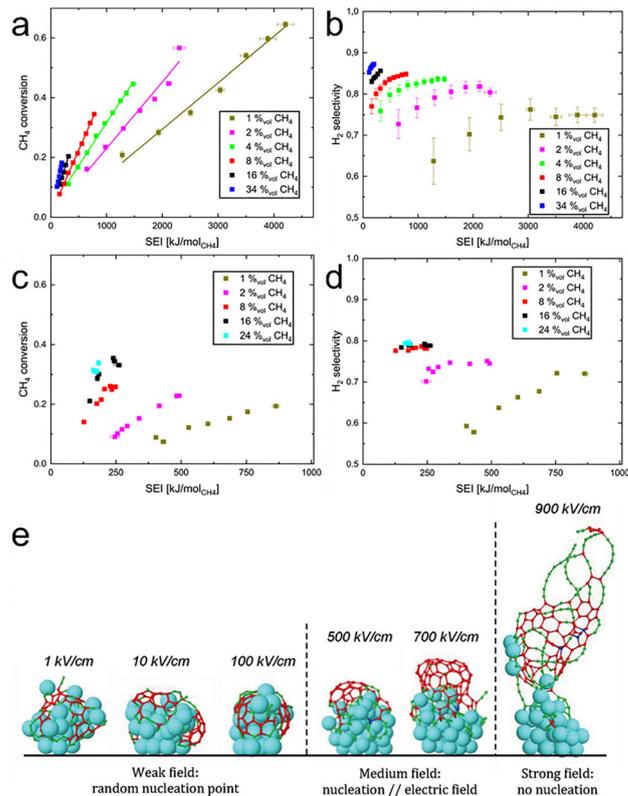

Fig. 7 (a) and (c) Methane conversion and (b) and (d) H_2 selectivity as a function of specific energy input (SEI) at varying methane dilution in (a) and (b) microwave plasma torch and (c) and (d) gliding arc plasmatron (GAP) reactor. Reproduced with permission from ref. 43. Copyright 2022 John Wiley and Sons. (e) Effect of electric field strength in plasma on carbon nanotube formation. Large atoms represent nickel atoms, red atoms represent 3-coordinated carbon network while green atoms represent 2- or 1-coordinated carbon networks. Reproduced with permission from ref. 119. Copyright 2012 American Chemical Society.

selectivity to H_2 in both plasma torch and GAP, which suggests the existence of complex kinetics at play (Fig. 7b and d). Specifically, the rate of carbon solid formation maximizes at 1900 K reaction temperature, and the competing side reactions of forming stable ethylene and acetylene are in the order of magnitude 6 times faster. As a result of smaller concentrations of hot (*i.e.*, 1900 K) zones in GAP than in the plasma torch configuration, lesser carbon solids are formed, and if formed, they are in the shape of amorphous spheres as opposed to graphitic carbon platelets in the plasma torch reaction.[43]

To a great extent, the reaction mechanisms involved in methane decomposition remain unclear even in conventional thermally driven processes, either with or without the presence of catalyst, let alone in the plasma-mediated reaction. Therefore, further in-depth studies are still required to fully unveil the reaction mechanism, possibly *via* the identification of carbon intermediates by *in situ* or *operando* techniques, to help researchers develop and optimize the system (of both the catalysts and/or plasma), as well as the appropriate operating parameters.

Plasma-catalysis for methane conversion to CNTs

Thermal plasmas ($>$4000 K) usually degrade catalysts, thus limiting plasma-catalysis integration to warm or non-thermal plasmas. In such systems, though product yields (H_2 and carbon) may decrease due to competing reactions, plasma-enhanced CVD (PECVD) has demonstrated success in synthesizing high-quality, vertically aligned CNTs.

CVD commonly requires ta gaseous carbon precursor, such as carbon monoxide, methane, acetylene, or liquid hydrocarbons and alcohols, or carbon clusters derived from solid carbon forms. Plasma can be seen as an "activator," where it is used to decompose and activate the gaseous precursor and is usually created by hot filaments (HF) or *via* electrical discharges such as DC, MW, or RF discharges.[120] In a general protocol, a thin layer of catalyst is usually applied onto a substrate, either prepared *via* a wet chemistry or sputtering process. The substrate is usually heated to somewhere between 650–1500 °C, where the reactive C species in the gaseous phase diffuse toward the substrate.[120] Therefore, CVD is still closely related to CDM as it also involves gaseous carbon precursor decomposition and growth of carbon on the catalyst surface. Additionally, PECVD is hitherto the most reliable technique to allow the control of alignment and orientation of the CNT bundles,[121] essentially because the electric field generated in the sheath region of the plasma aids in aligning the nanotubes.[122] Specifically, Bower *et al.* grew aligned CNTs on flat and bent surfaces, which is attributed to the presence of electrostatic self-bias at the surface.[123] In the presence of a metal catalyst (*i.e.*, nickel), the carbon atom attached to the nickel surface with a Ni–C bond would acquire a negative charge due to a charge transfer from nickel (*i.e.*, more electronegative) to carbon. The polarized carbon-nickel bond is thus subjected to migration by the electric field set up in PECVD, and supposed if the electric field strength is sufficiently strong enough to allow the migration to dominate thermal diffusion, the carbon cap can nucleate in parallel to the electric field to give a single-wall CNT[119] (Fig. 7e). However, if the electric field is too strong ($>$800 kV cm^{-1}), CNTs cannot be formed due to two opposing effects; a strong tendency for carbon atoms to nucleate on the catalytic surface (*i.e.*, enhanced binding strength between nickel and carbon) and the migration of charged carbon atoms away from the surface.

Apart from the CNT alignment, plasma, as mentioned earlier, functions like an "activator" because of the production of highly reactive species and partially dehydrogenated compounds for catalytic reactions. Not only plasma aided in lowering the activation barrier of dehydrogenation, plasma in PECVD was found to lower CNT growth activation barrier on nickel by $\sim$6 fold (*i.e.*, down from 1.2–1.5 eV to 0.23 eV).[124] It was hypothesized that the mechanism of carbon growth differs from that of conventional thermal CVD. For thermal CVD, CNT formation proceeds *via* a vapor–liquid–solid (VLS) mechanism, whereby after hydrocarbon gas adsorbs, catalytically decomposes, and diffuses in a metal particle, solid CNT forms after supersaturation and surface segregation.[125] On the other hand, CNT formation in PECVD is expected to be surface diffusion on solid metal catalysts and subsequent nucleation of carbon atoms at the edge of a CNT.[124]

To the best of our knowledge, there are few publications that have investigated the application of plasma-catalysis systems for methane decomposition (*i.e.*, plasma with catalyst packing).[115,116,126] As demonstrated by several studies on methane decomposition *via* thermal plasma, both carbon solids and hydrogen can be formed even in the absence of catalyst.[115,116,126] However, with the use of appropriate catalysts, the activation energy barrier of methane can be lowered. As demonstrated by the conventional catalyst designs, certain metal facets prefer carbon nucleation[127] that led to the formation of specific carbon products (*e.g.*, CNTs instead of CNFs or carbon black).[128] Ciobica *et al.* revealed from their *ab initio* studies of methane decomposition on a flat Ru surface (which is the (111) terrace site) that the methane preferably dissociates toward CH + 3H.[129] Bengaard *et al.* also observed similar effects on a flat Ni surface, although they also pointed out that the dissociation toward C + 4H preferably proceeds on a stepped Ni surface, suggesting that this site may be a possible carbon nucleation site.[130]

Although the combination between plasma and catalyst may not be commonly found for CDM or PECVD, several studies have highlighted the use of plasma as a medium for catalyst pretreatment prior to carrying out methane decomposition reaction. Plasma treating catalysts have been utilized to minimize sintering and agglomeration of active metal particles,[131] and in doing so, CNTs with smaller diameters were produced.[132] Plasma treatment with hydrogen-containing sources (*e.g.*, NH_3, H_2, *etc.*) could reduce metal oxides into their metallic states, and consequently improved the density and growth rate of carbon nanofibers at low temperature.[133,134] Catalyst pre-treatment by plasma may either offer beneficial or detrimental effects for catalysts prepared for CDM, depending on the intended objective. For example, Zhu *et al.* prepared Ni/Al_2O_3 *via* incipient wetness impregnation and treated the catalyst under argon glow discharge plasma for 1 h prior to calcination.[135] Interestingly, in contrast to the common expectation that plasma treatment enhances catalyst performance, the plasma-treated sample exhibited lower methane conversion than the untreated one. This discrepancy can be attributed to the increased presence of close-packed Ni crystal planes after plasma treatment, which are less favorable for methane activation compared to defect-rich sites.[136] Additionally, the plasma-treated catalyst showed lower carbon yield, likely due to its smaller Ni particle size (which hinders CNF formation)[137] and stronger metal-support interactions with Al_2O_3 (which suppress filamentous carbon detachment).[138,139] However, plasma-treated catalyst notably altered the carbon growth pathway, shifting from a mix of tip- and base-growth to predominantly base-growth, and influenced the tip structure of CNFs to be either open or closed (Fig. 8b and c, respectively).[135] This result highlights that plasma-based catalyst modification does not universally enhance CDM performance and can introduce both beneficial and detrimental changes depending on the metal dispersion, morphology, and metal–support interactions.
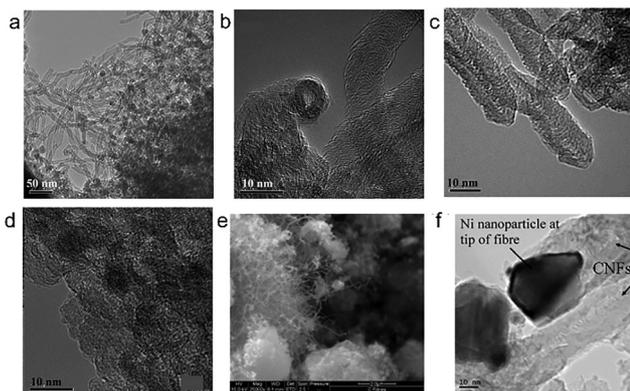
Fig. 8 TEM images of the carbon nanofibers produced at 500 °C using plasma-treated Ni/Al$_2$O$_3$, where (a) base-growth CNFs, (b) open tip CNFs, (c) closed tip CNFs, and (d) onion-like carbon formation. Reproduced with permission from ref. 135 Copyright 2008 Elsevier. (e) SEM and (f) TEM images of the produced CNFs from DBD plasma-assisted methane decomposition using Ni/Al$_2$O$_3$. Reproduced with permission from ref. 141 Copyright 2011 Elsevier.

Therefore, careful optimization of plasma conditions and catalyst structure is essential for achieving the desired performance.

Although plasma-catalytic CDM is less established than thermal CDM, studies using DBD plasmas with commercial NiO/Al$_2$O$_3$ catalysts demonstrated >99% H$_2$ selectivity and in situ NiO reduction at ~330 °C without external heating.[140,141] It has been proposed in a different work that in conventional high-temperature NiO reduction by CH$_4$, the reduction proceeds by the fragmentation of adsorbed CH$_4$ on the surface oxide active sites, forming active adsorbed carbon (C$_{ad}$) and H$_2$ as displayed by reactions. (R9)–(R15) as shown in Table 3 (with (R15) as the overall reaction).[142]

While in the plasma-catalytic reaction, it was found that there was quite a significant concentration of CH$_3$ and H formed, while lower amounts of CH$_2$ and CH are present; all formed via electron impact dissociations. In this case, radical recombination may occur to form higher hydrocarbons (resembling the NOCM process, which we will discuss in section "Plasma-assisted catalytic NOCM") or alternatively become adsorbed onto the surface of the catalyst. In the CDM mechanism, it is desirable to have higher hydrocarbons that can further fragment to form C$_{ad}$ and H$_2$, following reactions (R11)–(R15). As can be seen from Fig. 8e and f, some degree of filamentous carbon was formed, despite the predominantly undesirable tip-growth of carbon.[141]

Table 3 Mechanisms involved in methane decomposition to CNT provided by ref. 142

CH$_4$(g) → CH$_4$(ad)	(R9)
CH$_4$(ad) → CH$_3$(ad) + H(ad)	(R10)
CH$_3$(ad) → CH$_2$(ad) + H(ad)	(R11)
CH$_2$(ad) → CH(ad) + H(ad)	(R12)
CH(ad) → C$_{ad}$ + H(ad)	(R13)
2[2H(ad) → H$_2$(g)]	(R14)
CH$_4$(g) → C$_{ad}$ + 2H$_2$	(R15)

Plasma-assisted CDM enables simultaneous H$_2$ and CNT production, but its efficiency and controllability remain limited. Literature reveals that plasma lowers activation barriers and promotes CNT formation under milder conditions than thermal CVD, especially via PECVD. However, key challenges persist: (i) the mechanisms of CNT nucleation under plasma remain unclear, particularly the role of plasma-induced species and electric fields; (ii) energy efficiency is rarely benchmarked against thermal CDM or electrolysis, though warm plasma systems have shown promise in reducing power input; and (iii) CNT–catalyst separation is often not addressed—typical methods involve acid dissolution of metal particles or filtration, which may damage CNT quality or reduce economic viability. To address these gaps, future work should integrate in situ diagnostics (e.g., OES, DRIFTS), design recyclable catalyst supports, and conduct detailed energy audits under realistic operation to assess practical applicability.

Plasma-assisted catalytic NOCM

To compare plasma-catalytic and thermally driven NOCM, it is imperative that we first review the current research directions in thermal NOCM. The main challenge in catalyst design for NOCM is the difficulty in converting CH$_4$ directly due to the high energy for C–H bond activation (425 kJ mol^{-1}), large ionization energy, and low polarizability.[143] Therefore, current research has focused on the development of catalysts for selective C–H activation, and regulated C–C coupling catalysts have played a crucial role in the thermal NOCM process. The most effective catalysts contain the Fe supported on SiO$_2$ and zeolite catalysts, but the high selectivity catalysts at low temperatures still require more research.[144] Under thermal conditions, adsorbed species (C*, H*, CH*, CH$_2$*, and CH$_3$*) are key intermediates that participate in the coupling process, but conventional highly porous catalysts were reported as not effective for radical-based methane utilization due to their short mean free pathways in the gas phase. One of the most challenging aspects of NOCM is to control the structure of the catalyst to prevent coke formation due to the encapsulation of the catalyst particle from the formation of carbon solids.[145] To this end, synthesis strategies to induce high metal dispersion and confinement of metal sites, especially for iron-based SiO$_2$ catalysts, produce effective and stable catalysts for NOCM. Han et al. reported the Fe confined in cristobalite (CRS) Fe$\bigcirc$CRS (with confined labelled as '$\bigcirc$') catalyst with highly dispersed Fe carbide with Fe–Si coordination, which showed a high coke resistance due to the confined Fe sites being more favorable for methyl radical formation.[146] Furthermore, single iron sites embedded in a silica matrix enable high conversion to NOCM, and the lattice-confined Fe sites delivered a stable performance without deactivation after a 60 h time on stream.[147] Mechanistic studies using vacuum ultraviolet (VUV) synchrotron radiation to monitor the unconverted reactants, intermediates, and products of the Fe@SiO$_2$ catalyst, showed that the propargyl radicals were an essential precursor to synthesize aromatics for thermal NOCM.[144,148]

Extensive investigations have been focused on zeolite catalysts for NOCM reactions, Fe-based HZSM-5 zeolite is the most researched catalyst for this process, but it commonly exhibits a much lower activity and selectivity.[149] Liu *et al.* used Fe^{2+} exchanged HZSM-5 catalyst, and obtained a maximum selectivity of 75–80% to C_2 products at 15% CH_4 conversion.[150] Mo-modified HZSM-5 catalysts were also designed and developed to reduce carbon deposition. Miren *et al.* tuned the location of the evolving Mo species to understand their role in the catalytic activation and decay cycle, and found that the calcination step has been shown to regenerate and redistribute the Mo oxide species to create an active catalyst again.[151] Furthermore, the H_2 pre-treatment temperature could also be exploited to optimize the catalytic performance of the Mo/HZSM-5 catalyst.[152] Liu *et al.*[153] studied the effect of zeolite topology on carbon growth over Mo/MFI, Mo/MOR, Mo/BEA, and Mo/FAU templates, of which the Mo/BEA can perform best to achieve value-added carbon materials, hydrogen, light olefins, and aromatics. Noble metals could reach a considerable CH_4 conversion at lower temperatures, whereby using the alloy strategy not only promotes the activity but also decreases the cost. PtBi bimetallic alloy was supported on ZSM-5 zeolite and reached a high selectivity (>90%) to C_2 species at relatively moderate temperatures (600–700 °C).[154] Moreover, adding Sn as the promoter to Pt/SiO_2 or Pt/ZSM-5 catalysts not only resulted in a higher rate of ethylene formation but also increased the turnover frequency for the production of ethylene.[155]

While a general reaction mechanism for thermal-catalytic NOCM is still unclear as the reaction mechanism of the discovered active centers remains unknown, several studies have been carried out in an attempt to elucidate mechanistic insights on selected catalyst structures.[156,157] Li *et al.* analyzed the dynamic formation mechanism of $FeSiC_2\textcircled{C}SiO_2$ by density functional theory (DFT) and *ab initio* molecular dynamics (AIMD) simulations.[158] Furthermore, results from the AIMD simulations show that the dissociated methyl from methane prefers to move to the nearby carbon site at the $Fe\textcircled{C}SiC_2$ active center instead of desorbing into the gas phase, followed by C–C coupling and hydrogen to form the product *via* a key –CH–CH_2 intermediate.[159] Levin *et al.* proposed a catalytic cycle of $Ta_8O_2^+$ catalyst for the NOCM reaction (Fig. 9d) and revealed that the key step is product formation rather than C–H cleavages by kinetic isotope effect experiment.[160]

Aside from the design of selective catalytic sites for thermal NOCM, the utilization of plasma is another possible strategy for effective activation of the C–H bond in NOCM. Particular emphasis has been placed on the effects of vibrational excitation, electron impact dissociation and plasma generated radicals on the reaction mechanism under plasma conditions.[161,162] How does plasma-catalytic NOCM under the DBD plasma work? As shown as Fig. 10a and b, a schematic representation of streamer and reactive intermediates between dielectric particles due to an induced micro-electric field and the potential NOCM reaction pathway under the DBD plasma are illustrated. The local microelectric field between dielectric particles under an external electric field induces
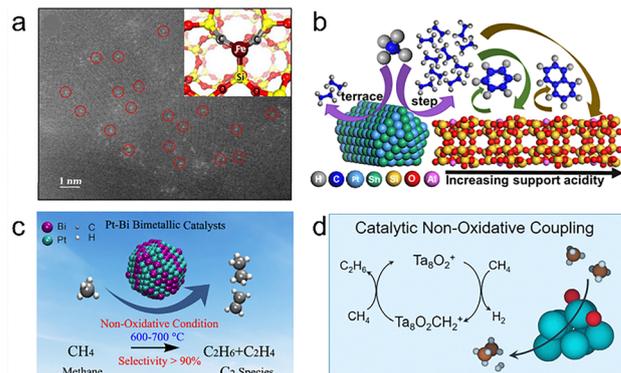

Fig. 9 (a) STEM-HAADF image of the $Fe@SiO_2$ catalyst with the inset showing the computational model,[148] (b) Pt–Bi bimetallic catalyst for NOCM,[154] (c) Pt–Sn/ZSM-5 catalysts for NOCM,[155] and (d) the mechanism of the $Ta_8O_2^+$ catalyst for the NOCM reaction.[160] Reprinted with permission from: (a) ref. 148 Copyright 2021 John Wiley and Sons; (b) ref. 154 Copyright 2018 American Chemical Society; (c) ref. 155 Copyright 2017 American Chemical Society; and (d) ref. 160 Copyright 2020 American Chemical Society.
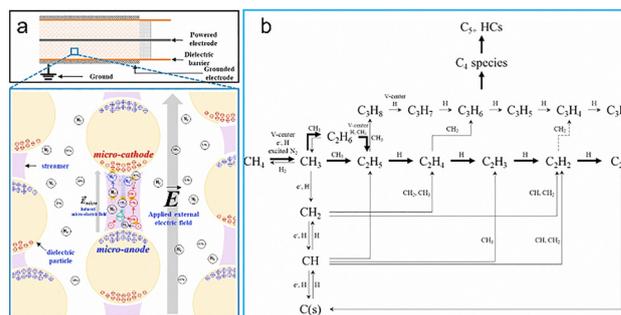

Fig. 10 (a) Schematic representation of streamer and reactive intermediates between dielectric particles due to induced micro-electric field and (b) the potential NOCM reaction pathway under the DBD plasma.[163] Copyright 2019 Elsevier.

polarization, leading to the generation and propagation of streamers and microdischarges, which drive ionization, electron avalanches, and sustain the discharge process through particle surface collisions, as described by a modified application of Paschen's equation.[163] In Yang's microkinetic study of a simulated NOCM process in DBD, it was shown that plasma-radicals generated upon electron impact dissociation play a larger role than vibrational excitation of methane in the absence of a catalyst, and the dominant reaction pathway is: CH_3^* is generated through electron impact dissociation (shown as (R16) in Table 3), followed by neutral-neutral recombination to from ethane (R17). However, tuning the selectivity of NOCM to ethylene *via* plasma power alone is difficult: at low specific energy input (SEI), electron energy is not sufficient to result in ethane dissociation (R18); conversely, at high SEI, high electron energy results in ethylene dissociation to acetylene (R19). Thus, achieving high ethylene selectivity is especially difficult to achieve under plasma-only conditions as it requires careful tuning of the electron energy. In general, the selective

production of valuable olefins from plasma-assisted NOCM is difficult to achieve under non-catalytic plasma conditions. To address the challenge of tuning product selectivity in plasma-assisted NOCM—particularly for ethylene—recent studies highlight the importance of electrode design, catalyst–plasma synergy, and process optimization. Tailored electrode configurations (e.g., packed-bed DBDs or needle–mesh systems) help localize discharges near catalyst surfaces, promoting CH_4 activation while limiting over-cracking.[164] Interface-engineered catalysts, such as Na_2WO_4–Mn_3O_4/m-SiO_2, have achieved up to 42% C_2 selectivity by stabilizing CH_x intermediates and confining reaction zones.[50] Additionally, optimizing specific energy input and introducing inert co-feeds (e.g., Ar, He) can extend radical lifetimes and favor C–C coupling pathways.[165,166]

Coupling plasma (especially NTP) with catalytic materials has the potential of achieving the benefits of high CH_4 conversion at temperatures below thermodynamic equilibrium and selective production of desirable C_{2+} products. The microkinetic modeling has theoretically revealed the efficacy of plasma in tuning the selectivity of different C_2 products using noble metals, while the impact of catalyst on the effectiveness of the plasma micro-discharges has been studied experimentally. Beyond the emphasis on elucidating reaction mechanisms and the design of catalytic sites for selective C–H breakage and C–C coupling in thermal NOCM, the focus in the plasma-catalytic NOCM section is to understand the synergistic interactions between plasma and catalysts (i.e., the effects of plasma in enhancing catalyst selectivity and vice versa) through mechanistic insights via both kinetic modelling and experimental studies demonstrating the effect of plasma–catalytic interactions on NOCM selectivity. Hence, in the following sections, we provide a summary of the mechanistic insights and catalyst design strategies reported in the current literature for plasma catalytic NOCM processes.

Mechanistic insights in plasma-catalytic NOCM

While mechanistic studies on plasma-catalytic NOCM have been limited, notable works by Engelmann et al., have utilized microkinetic modeling to mimic reaction conditions in a DBD reactor containing transition metal catalyst (e.g., Rh, Pt, Pd).[52] The authors developed a mean-field microkinetic model using microkinetic parameters from their previous literature for ammonia synthesis and oxidation,[22,167] coupled with DFT-derived activation energies from CatApp database,[168] to quantitatively investigate the effect of vibrational excitations and plasma radicals on the selectivity of C_2 hydrocarbon on various noble (e.g., Ru, Rh, Pt, Pd, Au, Ag) and non-noble metals (e.g., Cu) with a parameterized microkinetic model. To better appreciate the effect of plasma on the catalytic mechanisms in NOCM, pure thermal NOCM is simulated with 1 bar of CH_4 at 500 K on stepped sites of transition metals (i.e., (211)) (Fig. 11a). Turnover frequency (TOF) of NOCM revealed a volcano plot, with the Pd metal site giving the highest TOF at −0.1 eV. The rate-limiting step in the right flank of the volcano plot (i.e., weakly binding catalysts) is attributed to poor dissociation of the CH_4 reactant (i.e., $CH_4 \rightleftharpoons H + CH_3$). As for the left flank,
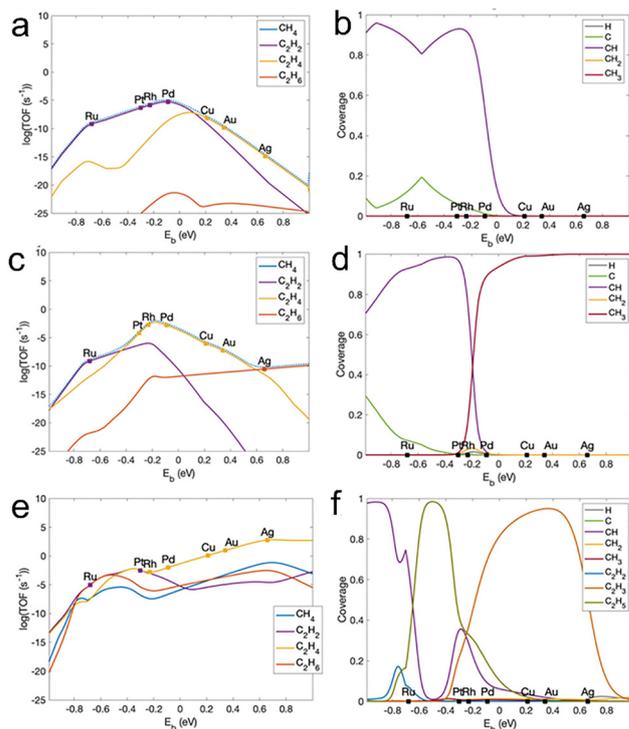

Fig. 11 (a), (c) and (e) Steady state turnover frequencies (TOFs) and (b), (d) and (f) species coverage on binding energies of CH_4 (E_b) for different metal step sites (211) for (a) and (b) thermal catalytic NOCM, (c) and (d) plasma catalytic NOCM with vibrationally excited CH_4, and (e) and (f) plasma catalytic NOCM with reactive radical species characteristic of a DBD plasma at 500 K.[52] Reproduced with permission from ref. 52 Copyright 2020 American Chemical Society.

methane conversion is instead inhibited by the rate of product formation (i.e., $C_2H_2^* \rightarrow C_2H_2(g)$) or coupling of CH* to give $C_2H_2^*$ for strongly binding catalysts. Dual volcano plots were observed for ethylene and ethane, which suggest the existence of two formation pathways, coupling and hydrogenation (e.g., ethylene; CH_2^* radicals coupling and hydrogenation of $C_2H_2^*$ to $C_2H_4^*$, ethane; CH_3^* radicals coupling and hydrogenation of $C_2H_4^*$ to $C_2H_6^*$; see Table 4 for a full list of elementary reaction steps). The active sites of the weakly binding catalysts were empty at steady state, as the coupling rate of dehydrogenated CH_3^* radical species (i.e., CH_2^* radicals) to $C_2H_4^*$ is faster than CH_4 dissociation (Fig. 11b). As for the stronger binding catalysts (i.e., Pd, Rh, Pt, and Ru), a non-negligible steady state coverage of CH* and C* is expected.

As plasma induces vibrationally excited methane, the authors modeled the energies of methane molecules with a Boltzmann distribution with a vibrational temperature of 1500 K, which, in theory, should give the highest TOF. In comparison with solely thermal NOCM, catalytic plasma NOCM, in the case of methane vibrational excitation, the main products shifted from acetylene (C_2H_2) to ethylene (C_2H_4) for the intermediate binding catalysts (i.e., Pt, Rh and Pd) (Fig. 11c). Ethylene and acetylene remain as the main products for the weakly binding catalysts (i.e., Cu, Au, and Ag) and the stronger binding catalyst (i.e., Ru), respectively. Vibrational excitation of methane

Table 4 List of reactions involving plasma radicals in NOCM under DBD plasma in the absence of catalyst[161]

Reaction		
Impact dissociation	$CH_4 + e^- \rightarrow CH_3\cdot + H\cdot + e^-$	(R16)
Ethane recombination	$CH_3\cdot + CH_3 \leftrightarrow C_2H_6$	(R17)
Ethane dissociation	$C_2H_6 + e^- \rightarrow C_2H_4 + H_2 + e^-$	(R18)
Ethylene dissociation	$C_2H_4 + e^- \rightarrow C_2H_2 + H_2 + e^-$	(R19)

Table 5 Elementary reaction steps involved in thermocatalytic methane decomposition and coupling reactions considered in the microkinetic model by Engelmann et al.[52]

Reaction step	Reaction equation
Adsorption/desorption	$H(g) + * \leftrightarrow H(g)*$
	$H_2(g) + 2* \leftrightarrow 2H*$
	$C(g) + * \leftrightarrow C*$
	$CH(g) +* \leftrightarrow CH*$
	$CH_2(g) + * \leftrightarrow CH_2*$
	$CH_3(g) + * \leftrightarrow CH_3*$
	$CH_4(g) + 2* \leftrightarrow 2CH_4*$
	$C_2H(g) + * \leftrightarrow C_2H*$
	$C_2H_2 + * \leftrightarrow C_2H_2*$
	$C_2H_3(g) + * \leftrightarrow C_2H_3*$
	$C_2H_4(g) + * \leftrightarrow C_2H_4*$
	$C_2H_5(g) + * \leftrightarrow C_2H_5*$
De-hydrogenation	$C* + H* \leftrightarrow CH* + *$
	$CH* + H* \leftrightarrow CH_2* + *$
	$CH_2* + H* \leftrightarrow CH_3* + *$
	$C_2H* + H* \leftrightarrow C_2H_2* + *$
	$C_2H_2* + H* \leftrightarrow C_2H_3* + *$
	$C_2H_3* + H* \leftrightarrow C_2H_4* + *$
	$C_2H_4* + H* \leftrightarrow C_2H_6(g) + 2*$
Carbon coupling	$2CH* \leftrightarrow C_2H_2* + *$
	$2CH_2* \leftrightarrow C_2H_4* + *$
	$2CH_3 \leftrightarrow C_2H_6(g) + 2*$

boosted methane conversion especially for the weakly binding metal sites that allowed for rapid coupling and desorption of dehydrogenated radicals as a result of rate-limiting methane dissociation. More notably, the formation of CH_3* on less active sites for thermal NOCM becomes easier when methane is vibrationally excited (Fig. 11d). Consequently, TOF for ethane formation increases by a factor 10^{12}. In the presence of plasma, radicals are formed due to electron impact dissociation, resulting in very different species (i.e., mainly C_2 species) having steady state coverage on metal active sites (Fig. 11f). Instead of $CH*$ and $C*$ typically observed for thermal and vibrationally excited NOCM for strong binding catalysts (i.e., Ru, Pt, Rh, Pd), C_2H_5*, C_2H_3* and $CH*$ are the main surface intermediates, and $CH*$ and C_2H_2* for the strongest binding catalyst (i.e., Ru). On the other hand, the surfaces of weakly binding catalysts (i.e., Cu, Au and Ag) would be saturated with C_2H_3*. The greater variety of surface intermediates is attributed to the presence of reactive H and H_2 in plasma that can further hydrogenate common $CH*$ and $C*$ surface species. However, this comes at the cost of selectivity toward a certain product (e.g., acetylene or ethylene). A good mix of C_2H_6, C_2H_4 and C_2H_2 is expected for strong binding catalysts (Fig. 11e), due to the difficult desorption of C_2H_2 which would break into $2CH*$ radicals. However, an advantage of plasma catalytic NOCM with radicals as opposed to thermal NOCM is the lower coke formation on catalytic surfaces at low operating temperatures. As the second-order hydrocarbon compounds (i.e., C_2H, C_2H_3 etc.) are already formed from radicalization in plasma, strong binding catalysts are not necessary for their formation. Coupled with the fact that $H*$ atoms are also in abundance, hydrogenation of these second-order compounds on the weak binding catalysts' surfaces can give rise to acetylene and ethylene. The reactions involving radicals induced by plasma dominate over conventional catalytic dissociation of methane, to give a plethora of intermediates or compounds that would not have been possible. More importantly, TOF of olefin (i.e., ethylene) can increase significantly when plasma-catalytic configuration is adopted, where higher selectivity to ethylene is observed for weak binding active sites (i.e., Ag) in high radical density plasma, and for intermediate binding catalysts (i.e., Pd and Cu) in high vibrational excitation plasma.

Microkinetic modeling, such as in the work of Engelmann et al., is indeed a promising scientific approach to understanding and improving plasma-catalytic system design (Table 5). Others can include detailed kinetic studies,[22,103,169] in situ/operando probing of plasma-activated species,[170] and atomistic simulations.[171] However, while simulations and modeling can provide significant insights, they may not corroborate well with empirical studies as the complex interactions between plasma and catalyst properties are neglected in kinetic models. Hu et al. studied NOCM in a DBD reactor with $0.5Pd/CeO_2$ catalysts and employed OES measurement and DFT calculations to explore the reaction mechanism for NOCM with the catalyst with and without plasma. Specifically, they have found that coking (i.e., catalyst deactivation) is more severe for the reaction without plasma on $0.5Pd/CeO_2$, where adsorbed CH_3* can undergo further dehydrogenation to $C*$ more easily (i.e., 1.02 eV) than desorption of CH_3* (i.e., 2.15 eV) (Fig. 12a). Whereas for the case of plasma, energetic electrons with sufficiently high energy (i.e., 55% of electrons with >2 eV at a reduced electric field intensity of $>100T_d$) can assist in the supposedly unfavorable desorption of the CH_3* for coupling to C_2H_6 in the gas phase. Subsequently, C_2H_6 will undergo dehydrogenation and recombination for ethylene and higher-order hydrocarbon formation (Fig. 12b).

Significant efforts have been made to uncover the mechanisms of NOCM in plasma (e.g., RF, MW, GA and DBD plasma) with vibrationally excited methane.[103,173,174] While there are no catalytic surface mechanisms simulated in those studies, plasma-induced mechanisms are still nevertheless valid due to the time-scale differences between plasma and catalyst-assisted reactions (Fig. 12c). The time-scale of the total catalytic surface reaction (i.e., chemisorption, surface rearrangement by spillover effect and surface diffusion, and diffusion of gaseous species) is in the range between 10^{-2} and 10^2 s, which is 2–3 orders of magnitude slower than the radical chemical reaction induced by plasma.[172] Hence, the catalytic surface reaction becomes the rate-limiting step for plasma-induced catalytic processes, which then becomes imperative for novel
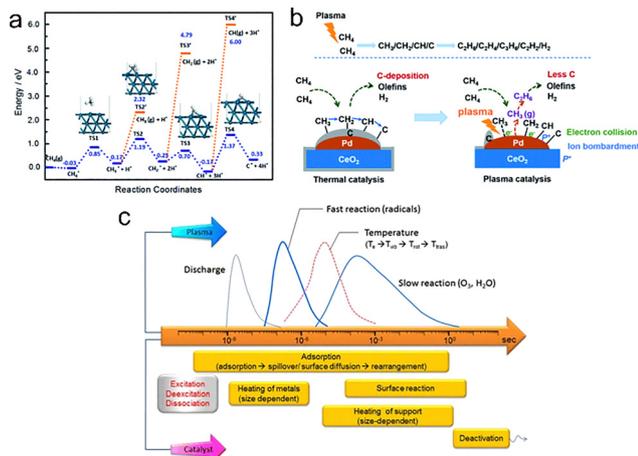
Fig. 12 (a) DFT calculations of consecutive pathways of CH_4 on a Pd-active site considering complete dehydrogenation (blue line) and desorption of reaction intermediates (orange line).[169] (b) Plausible mechanism pathway on Pd/CeO$_2$ with and without plasma in NOCM.[169] Reproduced with permission from ref. 169 Copyright 2022 Royal Society of Chemistry. (c) Characteristic time-scales for the plasma catalytic process.[172] Reproduced with permission from ref. 172 Copyright 2016 Springer.

technologies to study surface reactions *in situ*. Lee *et al.* designed a multimodal spectroscopy technique comprising polarization-modulation infrared reflection-absorption spectroscopy (PM-IRAS), mass spectrometry (MS), and optical emission spectroscopy (OES) to investigate plasma–surface reactions in NOCM.[170] The authors experimented on three different surfaces (*i.e.*, Ni, SiO$_2$, and KBr) with a DBD Ar plasma jet with CH_4 inflow at atmospheric temperature and pressure. Specifically, they found that the plasma-catalytic reaction in NOCM is likely to be a two-step process: (1) plasma-activated deposition, and (2) plasma-activated removal, instead of a simultaneous activation to produce olefins (*e.g.*, C=C compounds; ethylene). Ni investigated was the most active in forming carbonaceous surface deposits (*i.e.*, $CH_x{}^*$), and subsequently more C$_2$-species, C=C compounds and H$_2$ (Fig. 13a).[170] However, interestingly, NOCM with SiO$_2$ resulted in similar relative amounts of C$_2$-species and H$_2$ at attenuated amounts and the absence of any C=C compounds, which implies a very different coupling and hydrogenation process from that of Ni despite being still relatively active in plasma (Fig. 13b).[170] Diffuse reflectance infrared Fourier transform spectroscopy (DRIFTS) is also another plausible technique to investigate fundamental heterogeneous catalytic reactions,[175–177] but more importantly, *in situ* DRIFTS with a built-in plasma reactor can elucidate actual gaseous species and radicals adjacent to the catalyst surface in real-time.[178–181] Although such *in situ* or *operando* DRIFTS studies are rarely reported for the case of NOCM reactions and there are still fundamental plasma–surface interactions that are not yet fully discovered and understood for NOCM, more and more research developments in catalytic plasma surface science have been considered.

Operando DRIFTS has emerged as a vital tool for unraveling the reaction mechanisms of plasma-catalytic NOCM by
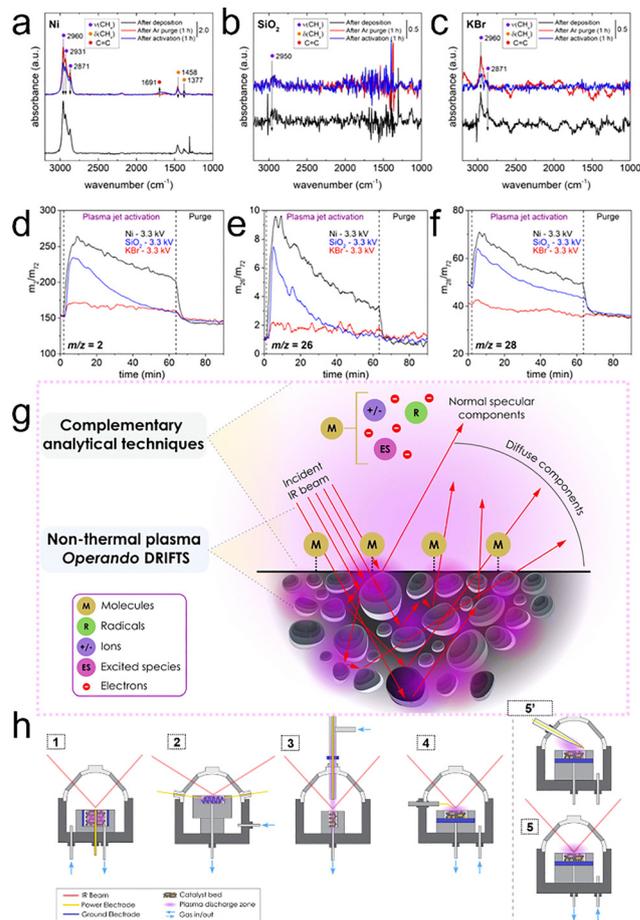

Fig. 13 Spectra of PM-IRAS and MS during plasma activation of carbonaceous deposits using Ar plasma jet (*i.e.*, ~20 kHz, peak-to-peak of 3.3 kV) at 298 K and 1 atm for 60 mins. PM-IRAS spectra of (a) Ni, (b) SiO$_2$, and (c) KBr for after depositing carbonaceous species on the surfaces with plasma activation of CH_4 (black line), after 1 h purging with Ar to remove unconverted CH_4 (red line), and after 1 h plasma activation of the carbonaceous deposits (blue line). Normalized MS spectra with pentane ($m/z = 72$) of (d) $m/z = 2$ representing H$_2$, (e) $m/z = 26$ and (f) $m/z = 28$ representing C$_2$ hydrocarbons, C$_2$H$_2$, C$_2$H$_4$ and C$_2$H$_6$ for Ni (black), SiO$_2$ (blue), and KBr (red) from during the 1 h plasma activation of the carbonaceous deposits. Reproduced with permission from ref. 170 Copyright 2021 American Chemical Society. Schematic (g) processes responsible for producing the diffuse reflected infrared spectrum of adsorbates on a powder catalyst and (h) *operando* DRIFTS configurations developed by research groups for investigating plasma catalysis under reaction conditions. Reproduced with permission from ref. 182 Copyright 2024 Elsevier.

identifying surface intermediates and tracking dynamic interactions between plasma-activated species and catalysts. Mukarakate *et al.* highlighted that future advancements should focus on optimizing DRIFTS cell designs for better integration with plasma zones, standardizing experimental protocols, and combining DRIFTS with complementary techniques like TPD, MS, and OES for comprehensive insights.[182] Herein, schematic processes responsible for producing the diffuse reflected infrared spectrum of adsorbates on a powder catalyst and *operando* DRIFTS configurations developed by Mukarakate's research group for investigating plasma catalysis under reaction

conditions are shown in Fig. 13g and h. These efforts will enable a deeper understanding of plasma–catalyst synergy, facilitate active site identification, and drive the design of efficient catalysts for sustainable methane conversion.

Hence, we herein highlight that limited information can be gained solely from theoretical studies and computational modeling. Not only are experimental validations important, but the effects of catalyst–plasma coupling (e.g., the effect of electrical properties of the catalyst on plasma) are not yet captured in computational chemical modeling. In this respect, the development and applications of in situ or operando techniques are extremely valuable. However, there are significant challenges present in applying these characterizations, including engineering new in situ sample holders or cells that are not commercially available.[183] Despite such challenges, some progress has been made in developing in situ and operando techniques to investigate the influence of plasma catalysis on methane conversion reactions; however, advancements remain limited, particularly in the context of plasma-catalytic methane decomposition.

Recent advances have demonstrated the potential of bifunctional tandem catalysts to enhance the efficiency and selectivity of plasma-assisted NOCM by separating activation and coupling functionalities into distinct domains. For instance, in a recent study by Li et al.,[50] a shielded bifunctional nanoreactor was constructed, wherein CH_4 molecules were first activated by an inner Ni–CeO_2 domain to form CH_x radicals under plasma, followed by controlled C–C coupling over an outer 2D Fe–Al_2O_3 shell. This spatial separation mitigated over-dehydrogenation and coke formation, while maintaining high ethylene selectivity. The mechanistic synergy was substantiated by in-situ DRIFTS and plasma OES, revealing enhanced concentrations of CH_3^* radicals and suppression of CH^* fragments associated with deep cracking. The bifunctional design highlights the importance of spatial and electronic separation of reaction sites to guide intermediate transformation under plasma, reinforcing the critical role of rational surface engineering in tuning product distribution for NOCM reactions.

Catalyst design for plasma-catalytic synergy for NOCM

While microkinetic models can elucidate mechanistic insights into plasma-activated catalysis, they often neglect plasma-catalysis synergistic interactions (i.e., effect of plasma on catalysts and the converse). In particular, dynamic changes to the catalyst (both active metals and supports) under the influence of plasma are usually observed.[184–186] Similarly, plasma itself may experience enhancements such as higher electron temperatures and effective electron impacts due to catalyst packing.[187] Experimental studies in plasma-catalytic NOCM have been conducted in NTPs such as gliding discharges and DBD reactors.[188–190] Notable studies by Jo et al. demonstrated the effects of electrical properties of Pt/Al_2O_3 and pure Al_2O_3 catalyst packing for CH_4 activation in a DBD reactor wherein methane conversion and selectivity to acetylene decreased for the packing with Pt.[188] The authors analyzed the effect of Pt

packing (modelled as 10 μm diameter spheres on 1 mm Al_2O_3 beads) on the Al_2O_3 by simulating the electric field distribution, which showed that the presence of the conductive Pt nanoparticles grounds the electrical field that reduces the overall electric field intensity within the DBD. An earlier study by Nozaki et al. reported that the dissociation of CH_3^* radicals decreases with electric field strength, which results in a lower density of CH^* and C^* radicals.[191] Consequently, the selectivity towards acetylene through CH^* recombination decreases with conductive catalyst packing. Kim et al. conducted a similar investigation on the effects of particle size of different dielectric packings (i.e., α-Al_2O_3, sand and KIT-6) for NOCM under DBD.[192] Their experimental results showed that smaller particles improve selectivity towards unsaturated C_2 hydrocarbons and selectivity toward total C_2 products, but catalyst material (i.e., dielectric properties) exhibited a relatively insignificant effect compared to particle size. The authors postulate that by reducing the particle size, the size of the gaps between each particle decreases, which leads to an increase in the number of effective collisions between radicals at the shorter gap distance, thus resulting in an increased probability of recombination of CH_2^* and CH^* radicals to form unsaturated C_2. Furthermore, experimental results have shown that the formation of coke decreases with decreasing particle size, indicating a greater tendency for dehydrogenation of hydrocarbon intermediates to coke at the interstitial gap between particles. The design of catalyst structure to hinder coke formation under plasma-driven NOCM has also been demonstrated by Liu et al. in their comparative study of atomically dispersed Pt over ceria (Pt/CeO_2-SAC) and nanoparticle Pt over ceria (Pt/CeO_2-NP),[105] in which the addition of Pt on ceria achieve higher CH_4 conversions and C_2 selectivity compared to pure plasma and ceria packing without Pt, possibly due to the generation of vibrationally excited methane species (that is nearly negligible in pure plasma) that results in the formation of C_2 intermediates on the Pt active sites. Consequently, Pt/CeO_2-SAC achieved higher CH_4 conversion and selectivity towards C_2 (Fig. 14a–c) due to higher dispersion of atomic Pt sites compared to Pt nanoparticles (i.e., Pt/CeO_2-NP) for C–H bond activation whereby the isolation of Pt atoms can hinder unselective coke formation.[192] In this study of plasma-catalytic NOCM reaction with single-atomic Pt catalyst, the bulk of the C_2 hydrocarbons formed are mainly C_2H_6 which follows predominantly impact dissociation (R16) and ethane recombination (R17), different from the expected higher yields of C_2H_4 hydrocarbon for the intermediate binding strength Pt catalyst via microkinetic modelling shown in Fig. 10c and e. Hence, profound plasma-catalytic synergy and mechanism remain to be fully understood for single-atom catalyst designs.

Aside from tuning catalysts to influence the plasma, modifications to the design of the reactor are another means of influencing catalyst–plasma interactions. Młotek et al. conducted NOCM reaction in a hybrid plasma-catalytic reactor system consisting of gliding arc discharge and mobile catalyst bed, demonstrating high selectivity towards C_2 products.[189] The presence of Pt and Pd in the mobile catalyst bed resulted in
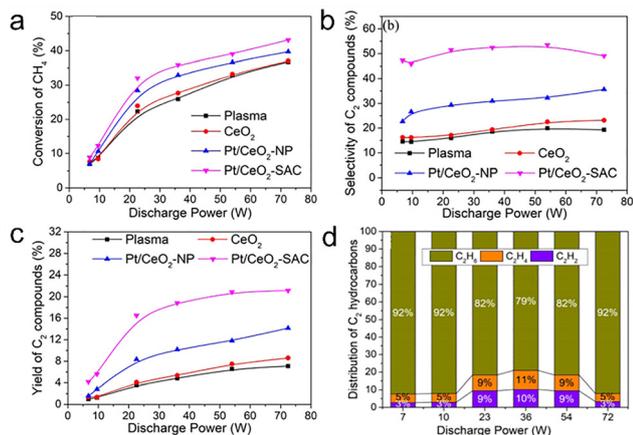
Fig. 14 Comparison of NOCM performance in DBD plasma without packing, with CeO₂, with Pt/CeO₂-SAC and Pt/CeO₂-NP by (a) CH₄ conversion, (b) C₂ selectivity, and (c) C₂ yield as a function of discharge power. (d) Distribution of normalized C₂ hydrocarbons for Pt/CeO₂-SAC as a function of discharge power. Reprinted with Permission from ref. 192 Copyright 2022 American Chemical Society.

an increased selectivity towards ethylene and ethane, which potentially suggests that the presence of catalyst sites promotes the hydrogenation of C_2H_2 to form ethane and ethylene as well as the recombination of CH_3^* and CH_2^* radicals. Nuria *et al.* investigated NOCM in a structured reactor with a catalytic layer of Pd/Al_2O_3,[193] and reported that the catalytic wall reactor achieved better C_2 selectivity and decreased unwanted carbon deposition compared to a fixed bed reactor with the same amount of catalyst packing. The authors proposed that the Pd/Al_2O_3 layer is able to better hydrogenate CH_x radicals with adsorbed H_2 species on the exposed surface, thus leading to greater selectivity toward C_2–C_4 hydrocarbons compared to a fixed bed reactor. These studies point to the potential innovations behind reactor engineering and design to tune the conversion and selectivity of NOCM through the plasma-catalysis interactions.

Plasma-assisted NOCM offers promising pathways for methane activation at low bulk temperatures *via* vibrational excitation and radical-mediated mechanisms, enabling higher olefin selectivity and reduced coke formation compared to thermal routes. Recent advances—such as bifunctional nanoreactor designs, single-atom catalysts, and tailored reactor configurations—demonstrate that spatial separation of activation and coupling sites, along with confinement effects, can mitigate over-dehydrogenation and enhance C–C coupling. However, key knowledge gaps remain, particularly regarding plasma–catalyst interfacial dynamics and product distribution control. Enhancing olefin selectivity requires synergistic control of radical generation (*via* plasma tuning), stabilization of CH_x intermediates (*via* catalyst design), and precise discharge localization (*via* reactor engineering). To address these challenges, integrated *in situ* techniques (*e.g.*, DRIFTS, OES), advanced modeling, and surface engineering strategies are essential to optimize selectivity, suppress coke, and guide future catalyst and reactor design.

Conclusions outlooks

Plasma-catalytic methane conversion presents a promising route for CO_x-free hydrogen production, CNTs, and high-value hydrocarbon synthesis. Advancing this field requires a comprehensive understanding of plasma–catalyst, plasma–substrate (reactant), and plasma–product interactions, along with optimized catalyst design and innovative reactor configurations. While microkinetic modeling provides insights into reaction mechanisms, experimental validation through *in situ* and *operando* techniques remains crucial.

Additionally, based on several surveyed snapshots, catalyst properties such as particle size and dielectric effects greatly influence plasma discharge behavior which impacts reaction selectivity. Therefore, future studies should focus on the impact of different plasma sources on catalyst performance, refining hybrid plasma–catalyst systems, and enhancing product selectivity. In particular, there is a growing need for novel catalyst designs tailored for plasma environments, moving beyond thermally derived materials. Such catalysts should be developed through a deeper understanding of gas-phase plasma chemistry, including the formation and lifetimes of vibrationally excited species, radicals, ions, and other plasma-induced intermediates across relevant spatial and temporal scales.

Research outlook on plasma-catalytic CDM processes

Based on what has been discussed for plasma-assisted CDM, the development of plasma-catalytic methane decomposition systems for high-throughput production of CNTs and hydrogen is not as well-established in the current literature as compared to related systems such as thermal plasma methane pyrolysis (without the presence of a catalyst) and PECVD. In PECVD, the growth of CNTs is prioritized over hydrogen production,[191] which makes it difficult to commercialize as a reliable production of H_2. Thermal plasma also has several bottlenecks: low H_2 energy yield and the need for a downstream H_2 purification unit.[14] In this regard, the design and engineering of plasma-catalytic methane decomposition systems are particularly important for the successful commercialization of such technologies for CO_x-free hydrogen production.

Research outlook in plasma-catalytic NOCM processes

To summarize our discussion on plasma-catalytic NOCM, while current research in designing effective thermal catalysts for NOCM has focused on designing active sites for C–H activation followed by selective C–C coupling (*e.g.*, the design of selective Fe©SiC₂ sites as previously mentioned), the design of optimal catalyst under plasma conditions requires careful consideration of the interaction between the plasma field and the material. On a fundamental level, microkinetic modeling studies such as Engelmann's can be utilized to investigate the combination of plasma effects and catalytic materials on the reaction mechanism, thus providing insights on the major

intermediates and rate-limiting steps involved in different catalytic metals (*e.g.*, for instance, showing that the selectivity towards ethylene can be increased with plasma radical density around weakly binding metals). While such mechanistic insights from kinetic modeling are elucidated from first principles by decoupling the effects of plasma-catalysis interactions, the role of plasma–catalyst synergy on the catalyst performance is often neglected in such models. To this end, *in situ* or *operando* techniques (*e.g.*, PM-IRAS in Lee *et al.*'s work) are imperative in facilitating the identification of important reaction pathways and intermediates from experiments in plasma-catalytic NOCM that are difficult to uncover from first-principle calculations.[170] Experimental studies have also elucidated the effect of catalyst properties (*e.g.*, particle size and dielectric properties) on the plasma discharge, and its consequent influence on the NOCM selectivity. As demonstrated by Liu *et al.*, creating highly dispersed metal sites is also a promising strategy to enhance olefin selectivity and in preventing coke formation under plasma conditions.[105] The design of the plasma-catalytic reactor configuration (*e.g.*, hybrid plasma–catalyst systems) also has the potential for optimizing the selectivity and conversion of plasma-catalytic NOCM. To successfully commercialize plasma-catalytic NOCM processes, each aspect of catalysis research and reaction engineering must be cohesively integrated. However, several critical challenges remain, including high energy consumption, limited product selectivity, catalyst deactivation, difficulties in reactor scale-up, and the lack of robust *in situ* diagnostics and process control, all of which must be systematically addressed to ensure industrial viability; mechanistic insights from fundamental studies in screening potential catalyst materials should be closely endorsed by the experimental studies, which could then shed light on the reaction mechanism and facilitate the optimization of catalyst properties; research into reactor design and engineering is also crucial for optimal scale-up of the reaction process. Future studies should investigate how various plasma sources impact catalyst properties during the NOCM process and, in turn, their selectivity activity.

Research outlook in coupling plasma-catalytic reactor with membrane separation

Though not deeply covered in this review, integrating plasma-catalysis with physical separation methods (such as membranes) has potential as a novel combinatory strategy to offer efficient and continuous product separation while ensuring process intensification. The membrane component selectively removes H_2 *in situ*, shifting the reaction equilibrium toward deeper CH_4 conversion and improving olefin selectivity *via* Le Chatelier's principle. The successful commercialization of these technologies depends on bridging fundamental research with experimental advancements, optimizing reactor design, and scaling up plasma-catalytic processes. In this final section before our concluding remarks, hence, we highlight the benefits of integrating a plasma-catalytic process with a membrane separator (*i.e.*, plasma-catalytic-membrane reactor) to achieve continuous production of value-added products (*i.e.*, CNTs *via* methane

decomposition or olefins from NOCM), and subsequent production of high-purity H_2.

The novel plasma–catalyst configuration was first conceptualized and developed by Mizushima *et al.*, where a membrane-like alumina tube was coated with catalyst particles as opposed to packing the reactor similar to that of a fixed-bed reactor, which is originally applied for ammonia synthesis.[194,195] A major advantage of this configuration is the facile separation of pure hydrogen gas. The appropriate design of this reactor is also expected to increase the efficiency of the plasma-chemical processes by: (1) placing the catalyst in the middle of the discharge zone, which is created between the inner and outer electrodes, (2) having small pores that could enhance the interaction between the catalyst and the vibrationally excited molecules generated, (3) allowing the selection of various catalysts to be integrated and coated on the membrane-like tube.[194] The original design of the reactor by Mizushima *et al.* is presented in Fig. 15.[194] Subsequent studies, such as by Chen *et al.*, also applied a similar configuration for CO_2 capture and utilization.[196]

More importantly, catalytic membrane reactors have several advantages over conventional thermochemical processes due to (1) facile and immediate separation of desirable products, (2) breaking thermodynamic conversion limits governed by Le Chatelier's principle, and (3) cost-effectiveness in a single-unit reactor design without requiring expensive separation processes (*e.g.*, cryogenic distillation, pressure swing adsorption, *etc.*).[197–200] However, there are no immediate commercial prospects in these catalytic membrane reactors due to the difficulty in developing stable catalytic membranes in harsh (high-temperature) thermochemical processes such as CDM and NOCM. Moreover, inorganic-based membrane supports are
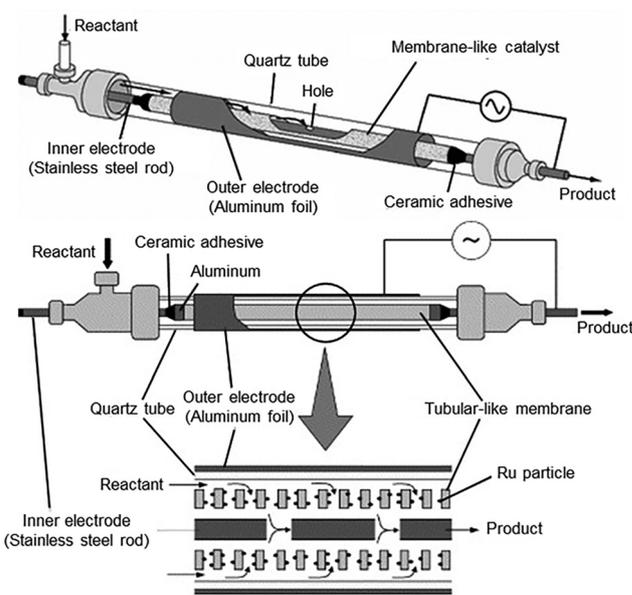

Fig. 15 Schematic diagram of a DBD plasma reactor coupled with a membrane-like catalyst. Reprinted with permission from ref. 194 and 195 Copyright 2004 Elsevier and 2006 Springer.

necessary for these processes, wherein cheaper alternatives like polymeric membranes (*i.e.*, two orders of magnitude lower[201]) would run the degradation risks.[198] Recently, our group has successfully designed a lab-scale catalytic membrane reactor, coupling Ni-SiO$_2$@CeO$_2$ core-shell catalyst with an ultra-thin Pd–Ag alloy membrane, for DRM reaction.[202,203] Our results demonstrated that by removing the hydrogen from the reaction stream, the methane conversion can be 1.5 higher than that without any membrane and the competing RWGS reaction could be drastically suppressed.[202] Catalytic membrane reactor designs were also successfully applied in other reactions (*i.e.*, hydrogen separation in propane dehydrogenation,[204,205] water separation in CO$_2$ hydrogenation to methanol,[206,207] carbon dioxide separation in shift reactions,[208] and oxygen separation in gasification reactions,[209] *etc.*).

In the case of plasma-catalytic processes, research and development of membranes under the influence of plasma is very scarce, with the plasma-catalytic membrane reactor designed by Mizushima *et al.* being one of the few reported studies. Herein, the membrane can be another useful factor to improve yields and selectivity of a desired product apart from tuning catalyst design strategies under plasma. The understanding and mechanistic insights of the role of adsorption, diffusion, or transportation mechanism of species in membrane under plasma, as well as the further development and engineering of membranes to withstand harsh plasma environments (*i.e.*, radical and ion bombardment), are foreseeable challenges to overcome.

Concluding remarks

In summary, we reviewed the current literature and recent advances on the application of plasma-catalysis systems for methane conversion reaction for CO$_x$-free H$_2$ production with a particular focus on methane decomposition and NOCM. While plasma-activation of methane can resolve the need for high-energy activation of C–H bonds, the governing reaction pathways and product selectivity are often difficult to tune with plasma power alone. Thus, coupling plasma with selected catalyst materials has been demonstrated to be effective in controlling the CNT morphology in CDM as well as C$_2$ selectivity in NOCM. In this regard, the current review gives an in-depth overview of the mechanistic insights and the synergistic interactions between catalysts and plasma in CO$_x$-free methane conversion *via* plasma-catalysis. As we have highlighted, there is still room for improvement for *in situ/operando* methods in revealing the direct experimental proof for the better understanding of plasma and catalyst synergy. While they are very useful for this purpose, often the setup is hindered by the difficulty in integrating the plasma sources and the diagnostic instrumentation itself. Nonetheless, several unique designs to circumvent this issue have emerged over the years as aforementioned in our review, which are gradually closing the gap between plasma and catalysis. Besides the mechanistic insights into plasma-catalysis systems for methane conversion, future

work would need to focus on reactor design and engineering to improve upon current technologies. A concept for a plasma-catalytic reactor with membrane separator configuration was also discussed herein as a potential implementation of a facile hydrogen production and purification unit, which could find the initial research basis for an efficient plasma-facilitated methane conversion.

Author contributions

Xiaohan Chen: conceptualization, data curation, writing – original draft, writing – review & editing, visualization, methodology; Bella: writing – original draft; Yifei Yue: writing – original draft; Mohammadreza Kosari: data curation, methodology, writing – review & editing; Lina Liu: writing – review & editing; Feiyang Hu: investigation; Keyu Cao: data curation; Yi Xiong: visualization; Aindrila Mandal: data curation; Jie Chang: writing – review & editing; Luwei Chen: writing – review & editing; Kang Hui Lim: writing – original draft, writing – review & editing, supervision, methodology; Sibudjing Kawi: writing – review & editing, supervision, project administration, funding acquisition.

Conflicts of interest

There are no conflicts to declare.

Data availability

No primary research results, software or code have been included and no new data were generated or analysed as part of this review.

Acknowledgements

References

1 J. A. Turner, *Science*, 2004, **305**, 972–974.
2 J. O. Bockris, *Int. J. Hydrogen Energy*, 2013, **38**, 2579–2588.
3 T. L. LeValley, A. R. Richard and M. Fan, *Int. J. Hydrogen Energy*, 2014, **39**, 16983–17000.

4 M. Shokrollahi, N. Teymouri, O. Ashrafi, P. Navarri and Y. Khojasteh-Salkuyeh, *Int. J. Hydrogen Energy*, 2024, **66**, 337–353.

5 Y. Li, Y. Tang, Y. Li and F. Tao, *Catal. Lett.*, 2023, **154**, 2140–2150.

6 C. Karakaya and R. J. Kee, *Prog. Energy Combust. Sci.*, 2016, **55**, 60–97.

7 R. Snoeckx, M. Setareh, R. Aerts, P. Simon, A. Maghari and A. Bogaerts, *Int. J. Hydrogen Energy*, 2013, **38**, 16098–16120.

8 Z. Li, L. Mo, Y. Kathiraser and S. Kawi, *ACS Catal.*, 2014, **4**, 1526–1536.

9 S. Kawi, Y. Kathiraser, J. Ni, U. Oemar, Z. Li and E. T. Saw, *ChemSusChem*, 2015, **8**, 3556–3575.

10 S. Das, J. Ashok, Z. Bian, N. Dewangan, M. Wai, Y. Du, A. Borgna, K. Hidajat and S. Kawi, *Appl. Catal., B*, 2018, **230**, 220–236.

11 Z. Bian, Z. Wang, B. Jiang, P. Hongmanorom, W. Zhong and S. Kawi, *Renewable Sustainable Energy Rev.*, 2020, **134**, 110291.

12 G. A. Olah, A. Goeppert, M. Czaun and G. K. Surya Prakash, *J. Am. Chem. Soc.*, 2013, **135**, 648–650.

13 Z. Li, Q. Lin, M. Li, J. Cao, F. Liu, H. Pan, Z. Wang and S. Kawi, *Renewable Sustainable Energy Rev.*, 2020, **134**, 110312.

14 N. Sánchez-Bastardo, R. Schlögl and H. Ruland, *Ind. Eng. Chem. Res.*, 2021, **60**, 11855–11881.

15 J. Kim, I. Choi and C. Chung, *Constr. Build. Mater.*, 2021, **302**, 124421.

16 D. Edlund, *Hydrogen and Syngas Production and Purification Technologies*, Wiley, 2009, pp. 357–384.

17 R. S. Postma, D. J. Keijsper, B. F. Morsink, E. H. Siegers, M. E. Mercimek, L. K. Nieukoop, H. van den Berg, A. G. van der Ham and L. Lefferts, *Ind. Eng. Chem. Res.*, 2021, **61**, 566–579.

18 T. Nozaki and K. Okazaki, *Catal. Today*, 2013, **211**, 29–38.

19 H. Mistry, A. S. Varela, C. S. Bonifacio, I. Zegkinoglou, I. Sinev, Y.-W. Choi, K. Kisslinger, E. A. Stach, J. C. Yang and P. Strasser, *Nat. Commun.*, 2016, **7**, 1–9.

20 S. Li, J. A. Medrano, V. Hessel and F. Gallucci, *Processes*, 2018, **6**, 248.

21 Z. Li, M. Li, J. Yang, M. Liao, G. Song, J. Cao, F. Liu, Z. Wang, S. Kawi and Q. Lin, *Catal. Today*, 2022, **388**, 12–25.

22 P. Mehta, P. Barboun, F. A. Herrera, J. Kim, P. Rumbach, D. B. Go, J. C. Hicks and W. F. Schneider, *Nat. Catal.*, 2018, **1**, 269–275.

23 M. Moreau, N. Orange and M. G. J. Feuilloley, *Biotechnol. Adv.*, 2008, **26**, 610–617.

24 R. Snoeckx and A. Bogaerts, *Chem. Soc. Rev.*, 2017, **46**, 5805.

25 X. Zhu, X. Gao, R. Qin, Y. Zeng, R. Qu, C. Zheng and X. Tu, *Appl. Catal., B*, 2015, **170–171**, 293–300.

26 H. Hosseini, *RSC Adv.*, 2023, **13**, 28211–28223.

27 E. B. Carolina, A. Garcia-Soto, T. Silva, V. Guerra, V. I. Parvulescu and O. Guaitella, *Plasma Chem. Plasma Process.*, 2024, **44**, 1287–1326.

28 S. Iijima, *Nature*, 1991, **354**, 56–58.

29 P. Zhang, C. Liang, M. Wu, X. Chen, D. Liu and J. Ma, *Energy Convers. Manage.*, 2022, **268**, 116017.

30 S. Van Alphen, F. Jardali, J. Creel, G. Trenchev, R. Snyders and A. Bogaerts, *Sustainable Energy Fuels*, 2021, **5**, 1786–1800.

31 H. Wang, J. Sun, Y. Li and W. Deng, *Sci. Data*, 2025, **12**, 648.

32 I. R. Hamdani, A. Ahmad, H. M. Chulliyil, C. Srinivasa-kannan, A. A. Shoaibi and M. M. Hossain, *ACS Omega*, 2023, **8**, 28945–28967.

33 H. Huang and L. Tang, *Energy Convers. Manage.*, 2007, **48**, 1331–1337.

34 F. Fabry, C. Rehmet, V. Rohani and L. Fulcheri, *Waste Biomass Valorization*, 2013, **4**, 421–439.

35 A. Fridman, *Plasma Chemistry*, Cambridge University Press, 2008.

36 K. S. Kim and T. H. Kim, *J. Appl. Phys.*, 2019, **125**, 070901.

37 S. Choi, T. H. Hwang, J. H. Seo, D. U. Kim and S. H. Hong, *IEEE Trans. Plasma Sci.*, 2004, **32**, 473–478.

38 H. Puliyalil, D. Lasic Jurkovic, V. Dasireddy and B. Likozar, *RSC Adv.*, 2018, **8**, 27481–27508.

39 J. Feng, X. Sun, Z. Li, X. Hao, M. Fan, P. Ning and K. Li, *Adv. Sci.*, 2022, **9**, e2203221.

40 A. George, B. Shen, M. Craven, Y. Wang, D. Kang, C. Wu and X. Tu, *Renewable Sustainable Energy Rev.*, 2021, **135**, 109702.

41 T. Nunnally, K. Gutsol, A. Rabinovich, A. Fridman, A. Gutsol and A. Kemoun, *J. Phys. D: Appl. Phys.*, 2011, **44**, 274009.

42 M. Jasiński, D. Czylkowski, B. Hrycak, M. Dors and J. Mizeraczyk, *Int. J. Hydrogen Energy*, 2013, **38**, 11473–11483.

43 S. Kreuznacht, M. Purcel, S. Böddeker, P. Awakowicz, W. Xia, M. Muhler, M. Böke and A. V. Keudell, *Plasma Processes Polym.*, 2022, e2200132.

44 V. Maslova, R. Nastase, G. Veryasov, N. Nesterenko, E. Fourré and C. Batiot-Dupeyrat, *Prog. Energy Combust. Sci.*, 2024, **101**, 101096.

45 E. Morais, E. Delikonstantis, M. Scapinello, G. Smith, G. D. Stefanidis and A. Bogaerts, *Chem. Eng. J.*, 2023, **462**, 142227.

46 L. Lefferts, *Angew. Chem., Int. Ed.*, 2024, **136**, e202305322.

47 J. Slaets, B. Loenders and A. Bogaerts, *Fuel*, 2024, **360**, 130650.

48 J. Sun, Q. Chen, W. Qin, H. Wu, B. Liu, S. Li and A. Bogaerts, *Chem. Eng. J.*, 2024, **498**, 155847.

49 P. N. Kechagiopoulos, J. Rogers, P.-A. Maitre, A. J. McCue and M. N. Bannerman, *Plasma Chem. Plasma Process.*, 2024, **44**, 2057–2085.

50 C. Lu, Y. Wang, D. Tian, R. Xu, R. J. Wong, S. Xi, W. Liu, H. Wang, X. Tu and K. Li, *Nat. Commun.*, 2025, **16**, 4585.

51 T. Zhu, C. Li, X. Zhang, B. Yuan, M. Wang, X. Zhang, X. Xu and Q. Sun, *Atmosphere*, 2025, **16**, 376.

52 Y. Engelmann, P. Mehta, E. C. Neyts, W. F. Schneider and A. Bogaerts, *ACS Sustainable Chem. Eng.*, 2020, **8**, 6043–6054.

53 P. A. Maitre, M. S. Bieniek and P. N. Kechagiopoulos, *J. Phys. Chem. C*, 2022, **126**, 19987–20003.

54 Z. Chen, S. Wu, J. Ma, S. Mine, T. Toyao, M. Matsuoka, L. Wang and J. Zhang, *Angew. Chem., Int. Ed.*, 2021, **60**, 11901–11909.

55 S. Chen, S. Li, R. You, Z. Guo, F. Wang, G. Li, W. Yuan, B. Zhu, Y. Gao, Z. Zhang, H. Yang and Y. Wang, *ACS Catal.*, 2021, **11**, 5666–5677.

56 R. Liu, E. Morais, D. Li, P. Liu, Q. Chen, S. Li, L. Wang, X. Gao, A. Bogaerts, H. Guo and Y. Yi, *Chem. Eng. J.*, 2024, **498**, 155733.

57 Y. Guan, G. Song, C. Li, K. H. Lim, B. Wang, L. Xia, H. Song, Y. Liu, C. Wu and S. Kawi, *Carbon Capture Sci. Technol.*, 2024, **11**, 100200.

58 B. Wang, B. Chen, Y. Sun, H. Xiao, X. Xu, M. Fu, J. Wu, L. Chen and D. Ye, *Appl. Catal., B*, 2018, **238**, 328–338.

59 X. Yan, B. Zhao, Y. Liu and Y. Li, *Catal. Today*, 2015, **256**, 29–40.

60 T. M. Gür, *Chem. Rev.*, 2013, **113**, 6179–6206.

61 P. Tang, Q. Zhu, Z. Wu and D. Ma, *Energy Environ. Sci.*, 2014, **7**, 2580–2591.

62 R. M. Navarro, M. A. Pena and J. L. G. Fierro, *Chem. Rev.*, 2007, **107**, 3952–3991.

63 J. Ashok, S. Pati, P. Hongmanorom, T. Zhang, J. Chen and S. Kawi, *Catal. Today*, 2020, **356**, 471–489.

64 Z. Bian, Y. M. Chan, Y. Yu and S. Kawi, *Catal. Today*, 2020, **347**, 31–38.

65 A. Jangam, S. Das, N. Dewangan, P. Hongmanorom, W. M. Hui and S. Kawi, *Catal. Today*, 2020, **358**, 3–29.

66 S. Kawi, J. Ashok, N. Dewangan, S. Pati and J. Chen, *Waste Biomass Valorization*, 2021, 1–30.

67 T. Maneerung, J. Liew, Y. Dai, S. Kawi, C. Chong and C. H. Wang, *Bioresour. Technol.*, 2016, **200**, 350–359.

68 J. Ashok and S. Kawi, *ACS Catal.*, 2014, **4**, 289–301.

69 S. Das, K. H. Lim, T. Z. H. Gani, S. Askari and S. Kawi, *Appl. Catal., B*, 2023, **323**, 122141.

70 Z. Wang, Z. Li, Y. Cui, T. Chen, J. Hu and S. Kawi, *Environ. Sci. Technol.*, 2019, **53**, 9937–9946.

71 N. Dewangan, M. H. Wai, S. Jayaprakash, A.-R. Bawah, A. J. Poerjoto, T. Jie, J. Ashok, K. Hidajat and S. Kawi, *Catal. Today*, 2020, **356**, 490–513.

72 X. Gao, Z. Tan, K. Hidajat and S. Kawi, *Catal. Today*, 2017, **281**, 250–258.

73 X. Pan, F. Jiao, D. Miao and X. Bao, *Chem. Rev.*, 2021, **121**, 6588–6609.

74 F. Pöhlmann and A. Jess, *Catal. Today*, 2016, **275**, 172–182.

75 C. Kibby, K. Jothimurugesan, T. Das, H. S. Lacheen, T. Rea and R. J. Saxton, *Catal. Today*, 2013, **215**, 131–141.

76 A. Holmen, *Catal. Today*, 2009, **142**, 2–8.

77 M. Li, Z. Li, Q. Lin, J. Cao, F. Liu, M. H. Wai and S. Kawi, *Catal. Today*, 2022, **402**, 319–327.

78 D. L. Sun, F. Wang, R. Y. Hong and C. R. Xie, *Diamond Relat. Mater.*, 2016, **61**, 21–31.

79 J. L. Figueiredo, C. A. Bernardo, J. J. Chludzinski Jr and R. T. K. Baker, *J. Catal.*, 1988, **110**, 127–138.

80 T. Maneerung, K. Hidajat and S. Kawi, *Int. J. Hydrogen Energy*, 2015, **40**, 13399–13411.

81 J. Raza, A. H. Khoja, M. Anwar, F. Saleem, S. R. Naqvi, R. Liaquat, M. Hassan, R. Javaid, U. Y. Qazi and B. Lumbers, *Renewable Sustainable Energy Rev.*, 2022, **168**, 112774.

82 X. Zhao, S. Sun, F. Yang and Y. Li, *Acc. Chem. Res.*, 2022, **55**, 3334–3344.

83 A. Javey, J. Guo, Q. Wang, M. Lundstrom and H. Dai, *Nature*, 2003, **424**, 654–657.

84 R. Andrews, D. Jacques, D. Qian and T. Rantell, *Acc. Chem. Res.*, 2002, **35**, 1008–1017.

85 H. F. Abbas and W. M. A. Wan Daud, *Int. J. Hydrogen Energy*, 2010, **35**, 1160–1190.

86 W. Henao, F. Cazaña, P. Tarifa, E. Romeo, N. Latorre, V. Sebastian, J. J. Delgado and A. Monzón, *Chem. Eng. J.*, 2021, **404**, 126103.

87 I. Amghizar, L. A. Vandewalle, K. M. Van Geem and G. B. Marin, *Engineering*, 2017, **3**, 171–178.

88 Y. Gao, L. Neal, D. Ding, W. Wu, C. Baroi, A. M. Gaffney and F. Li, *ACS Catal.*, 2019, **9**, 8592–8621.

89 C. Guéret, M. Daroux and F. Billaud, *Chem. Eng. Sci.*, 1997, **52**, 815–827.

90 K. Huang, J. B. Miller, G. W. Huber, J. A. Dumesic and C. T. Maravelias, *Joule*, 2018, **2**, 349–365.

91 J. R. Rose, *US Pat.*, US1352085A, 1920.

92 J. Fincke, R. Anderson, T. Hyde and B. Detering, *Ind. Eng. Chem. Res.*, 2002, **41**, 1425–1435.

93 C. L. Cheung, A. Kurtz, H. Park and C. M. Lieber, *J. Phys. Chem. B*, 2002, **106**, 2429–2433.

94 T. Guo, P. Nikolaev, A. Thess, D. T. Colbert and R. E. Smalley, *Chem. Phys. Lett.*, 1995, **243**, 49–54.

95 I. A. Novoselova, N. F. Oliinyk, S. V. Volkov, A. A. Konchits, I. B. Yanchuk, V. S. Yefanov, S. P. Kolesnik and M. V. Karpets, *Phys. E*, 2008, **40**, 2231–2237.

96 A. Caballero and P. J. Perez, *Chem. Soc. Rev.*, 2013, **42**, 8809–8820.

97 K. H. R. Rouwenhorst, H.-H. Kim and L. Lefferts, *ACS Sustainable Chem. Eng.*, 2019, **7**, 17515–17522.

98 E. C. Neyts, K. Ostrikov, M. K. Sunkara and A. Bogaerts, *Chem. Rev.*, 2015, **115**, 13408–13446.

99 J. C. Whitehead, in *Plasma Catalysis: Fundamentals and Applications*, ed. X. Tu, J. C. Whitehead and T. Nozaki, Springer Cham, Switzerland, 2019, DOI: 10.1007/978-3-030-05189-1.

100 K. H. Lim, Y. Yue, Bella, X. Gao, T. Zhang, F. Hu, S. Das and S. Kawi, *ACS Sustainable Chem. Eng.*, 2023, **11**, 4903–4933.

101 T. Li, C. Rehmet, Y. Cheng, Y. Jin and Y. Cheng, *Plasma Chem. Plasma Process.*, 2017, **37**, 1033–1049.

102 F. Kerscher, A. Stary, S. Gleis, A. Ulrich, H. Klein and H. Spliethoff, *Int. J. Hydrogen Energy*, 2021, **46**, 19897–19912.

103 J. Sun and Q. Chen, *J. Energy Chem.*, 2019, **39**, 188–197.

104 M. Heintze, M. Magureanu and M. Kettlitz, *J. Appl. Phys.*, 2002, **92**, 7022–7031.

105 L. Liu, S. Das, Z. Zhang and S. Kawi, *ACS Appl. Mater. Interfaces*, 2022, **14**, 5363–5375.

106 G. Chen, X. Tu, G. Homm and A. Weidenkaff, *Nat. Rev. Mater.*, 2022, **7**, 333–334.

107 S. Timmerberg, M. Kaltschmitt and M. Finkbeiner, *Energy Convers. Manage.*, 2020, **7**, 100043.

108 G. B. Skinner and R. A. Ruehrwein, *J. Phys. Chem.*, 1959, **63**, 1736–1742.

109 C. J. Chen, M. H. Back and R. A. Back, in *Industrial and Laboratory Pyrolyses*, ed. L. F. Albright and B. L. Crynes, American Chemical Society, Washington, DC, 1976, vol. 32, ch. 1, pp. 1–16.

110 V. Kevorkian, C. E. Heath and M. Boudart, *J. Phys. Chem.*, 1960, **64**, 964–968.

111 G. I. Kozlov and V. G. Knorre, *Combust. Flame*, 1962, **6**, 253–263.

112 M. S. Khan and B. L. Crynes, *Ind. Eng. Chem. Res.*, 1970, **62**, 54–59.

113 S. Timmerberg, M. Kaltschmitt and M. Finkbeiner, *Energy Convers. Manage.: X*, 2020, **7**, 100043.

114 X. Meng, X. Cui, N. Pethan Rajan, L. Yu, D. Deng and X. Bao, *Chem*, 2019, **5**, 2296–2325.

115 M. Gautier, V. Rohani and L. Fulcheri, *Int. J. Hydrogen Energy*, 2017, **42**, 28140–28156.

116 L. Fulcheri, V.-J. Rohani, E. Wyse, N. Hardman and E. Dames, *Int. J. Hydrogen Energy*, 2023, **48**, 2920–2928.

117 E. Dames and H. Wang, *Proc. Combust. Inst.*, 2013, **34**, 307–314.

118 A. Violi, A. D'Anna and A. D'Alessio, *Chem. Eng. Sci.*, 1999, **54**, 3433–3442.

119 E. C. Neyts, A. C. T. van Duin and A. Bogaerts, *J. Am. Chem. Soc.*, 2012, **134**, 1256–1260.

120 M. L. Terranova, V. Sessa and M. Rossi, *Chem. Vap. Deposition*, 2006, **12**, 315–325.

121 G. S. Duesberg, A. P. Graham, F. Kreupl, M. Liebau, R. Seidel, E. Unger and W. Hoenlein, *Diamond Relat. Mater.*, 2004, **13**, 354–361.

122 M. S. Bell, K. B. K. Teo, R. G. Lacerda, W. I. Milne, D. B. Hash and M. Meyyappan, *Pure Appl. Chem.*, 2006, **78**, 1117–1125.

123 C. Bower, W. Zhu, S. Jin and O. Zhou, *Appl. Phys. Lett.*, 2000, **77**, 830–832.

124 S. Hofmann, B. Kleinsorge, C. Ducati, A. C. Ferrari and J. Robertson, *Diamond Relat. Mater.*, 2004, **13**, 1171–1176.

125 R. T. K. Baker, M. A. Barber, P. S. Harris, F. S. Feates and R. J. Waite, *J. Catal.*, 1972, **26**, 51–62.

126 T. Li, C. Rehmet, Y. Cheng, Y. Jin and Y. Cheng, *Plasma Chem. Plasma Process.*, 2017, **37**, 1033–1049.

127 S. Esconjauregui, C. M. Whelan and K. Maex, *Carbon*, 2009, **47**, 659–669.

128 X. Lim, S. Low and W. Oh, *Fuel Process. Technol.*, 2023, **241**, 107624.

129 I. M. Ciobica and R. A. van Santen, *J. Phys. Chem. B*, 2002, **106**, 6200–6205.

130 H. S. Bengaard, J. K. Nørskov, J. Sehested, B. S. Clausen, L. P. Nielsen, A. M. Molenbroek and J. R. Rostrup-Nielsen, *J. Catal.*, 2002, **209**, 365–384.

131 X. Gao, Z. Lin, T. Li, L. Huang, J. Zhang, S. Askari, N. Dewangan, A. Jangam and S. Kawi, *Catalysts*, 2021, **11**, 455.

132 Z. Ghorannevis, T. Kato, T. Kaneko and R. Hatakeyama, *J. Am. Chem. Soc.*, 2010, **132**, 9570–9572.

133 A. Malesevic, H. Chen, T. Hauffman, A. Vanhulsel, H. Terryn and C. V. Haesendonck, *Nanotechnology*, 2007, **18**, 455602.

134 M. Cantoro, S. Hofmann, C. Mattevi, S. Pisana, A. Parvez, A. Fasoli, C. Ducati, V. Scardaci, A. C. Ferrari and J. Robertson, *J. Appl. Phys.*, 2009, **105**, 064304.

135 X. Zhu, D. Cheng and P. Kuai, *Energy Fuels*, 2008, **22**, 1480–1484.

136 X. Zhu, Y. Zhang and C. Liu, *Catal. Lett.*, 2007, **118**, 306–312.

137 D. Chen, K. O. Christensen, E. Ochoa-Fernández, Z. Yu, B. Tøtdal, N. Latorre, A. Monzón and A. Holmen, *J. Catal.*, 2005, **229**, 82–96.

138 X. Li, Y. Zhang and K. J. Smith, *Appl. Catal., A*, 2004, **264**, 81–91.

139 X. Gao, J. Ashok and S. Kawi, *Catal. Today*, 2022, **397**, 581–591.

140 Z. Luo, S. Lim, Y. You, J. Miao, H. Gong, J. Zhang, S. Wang, J. Lin and Z. Shen, *Nanotechnology*, 2008, **19**, 255607.

141 H. J. Gallon, X. Tu, M. V. Twigg and J. C. Whitehead, *Appl. Catal., B*, 2011, **106**, 616–620.

142 R. Alizadeh, E. Jamshidi and H. Ale Ebrahim, *Chem. Eng. Technol.*, 2007, **30**, 1123–1128.

143 D. Bajec, A. Kostyniuk, A. Pohar and B. Likozar, *Chem. Eng. J.*, 2020, **396**, 125182.

144 Z. Chen, S. Wu, J. Ma, S. Mine, T. Toyao, M. Matsuoka, L. Wang and J. Zhang, *Angew. Chem., Int. Ed.*, 2021, **60**, 11901–11909.

145 A. L. Dipu, S. Ohbuchi, Y. Nishikawa, S. Iguchi, H. Ogihara and I. Yamanaka, *ACS Catal.*, 2019, **10**, 375–379.

146 S. J. Han, S. W. Lee, H. W. Kim, S. K. Kim and Y. T. Kim, *ACS Catal.*, 2019, **9**, 7984–7997.

147 X. Guo, G. Fang, G. Li, H. Ma, H. Fan, L. Yu, C. Ma, X. Wu, D. Deng, M. Wei, D. Tan, R. Si, S. Zhang, J. Li, L. Sun, Z. Tang, X. Pan and X. Bao, *Science*, 2014, **344**, 616–619.

148 A. Puente-Urbina, Z. Pan, V. Paunovic, P. Sot, P. Hemberger and J. A. van Bokhoven, *Angew. Chem., Int. Ed.*, 2021, **60**, 24002–24007.

149 V. Abdelsayed, D. Shekhawat and R. S. Tempke, *Catal. Today*, 2021, **365**, 88–102.

150 Y. Xu, X. Yuan, M. Chen, A. Dong, B. Liu, F. Jiang, S. Yang and X. Liu, *J. Catal.*, 2021, **396**, 224–241.

151 M. Agote-Arán, A. B. Kroner, H. U. Islam, W. A. Sławiński, D. S. Wragg, I. Lezcano-González and A. M. Beale, *ChemCatChem*, 2018, **11**, 473–480.

152 Á. López-Martín, A. Caballero and G. Colón, *Appl. Catal., B*, 2022, **312**, 121382.

153 Y. Liu, E. H. Osta, A. S. Poryvaev, M. V. Fedin, A. Longo, A. Nefedov and N. Kosinov, *Carbon*, 2023, **201**, 535–541.

154 Y. Xiao and A. Varma, *ACS Catal.*, 2018, **8**, 2735–2740.

155 D. Gerceker, A. H. Motagamwala, K. R. Rivera-Dones, J. B. Miller, G. W. Huber, M. Mavrikakis and J. A. Dumesic, *ACS Catal.*, 2017, **7**, 2088–2100.

156 M. Yoshida, Y. Tsuji, S. Iguchi, H. Nishiguchi, I. Yamanaka, H. Abe, T. Kamachi and K. Yoshizawa, *ACS Catal.*, 2022, **12**, 9458–9472.

157 J. Hao, P. Schwach, G. Fang, X. Guo, H. Zhang, H. Shen, X. Huang, D. Eggart, X. Pan and X. Bao, *ACS Catal.*, 2019, **9**, 9045–9050.

158 T.-H. Li, M. Yan, Y. Liu, Z.-Q. Huang, C.-R. Chang and J. Li, *J. Phys. Chem. C*, 2020, **124**, 13656–13663.

159 Y. Liu, J. C. Liu, T. H. Li, Z. H. Duan, T. Y. Zhang, M. Yan, W. L. Li, H. Xiao, Y. G. Wang, C. R. Chang and J. Li, *Angew. Chem., Int. Ed.*, 2020, **59**, 18586–18590.

160 N. Levin, J. Lengyel, J. F. Eckhard, M. Tschurl and U. Heiz, *J. Am. Chem. Soc.*, 2020, **142**, 5862–5869.

161 Y. Yang, *Plasma Chem. Plasma Process.*, 2003, **23**, 327–346.

162 Y. Yang, *Plasma Chem. Plasma Process.*, 2003, **23**, 283–296.

163 J. Kim, J. Jeoung, J. Jeon, J. Kim, Y. S. Mok and K.-S. Ha, *Chem. Eng. J.*, 2019, **377**, 119896.

164 T. S. Larsen, J. A. Andersen, J. M. Christensen, A. Fateev, M. Østberg, E. Morais, A. Bogaerts and A. D. Jensen, *Plasma Chem. Plasma Process.*, 2025, **45**, 843–871.

165 V. Longo, L. De Pasquale, S. Perathoner, G. Centi and C. Genovese, *Catal. Sci. Technol.*, 2025, **15**, 3725–3735.

166 R. Liu, Y. Hao, T. Wang, L. Wang, A. Bogaerts, H. Guo and Y. Yi, *Chem. Eng. J.*, 2023, **463**, 142442.

167 H. Ma and W. F. Schneider, *ACS Catal.*, 2019, **9**, 2407–2414.

168 J. S. Hummelshøj, F. Abild-Pedersen, F. Studt, T. Bligaard and J. K. Nørskov, *Angew. Chem., Int. Ed.*, 2012, **51**, 272–274.

169 X. Hu, Y. Liu, L. Dou, C. Zhang, S. Zhang, Y. Gao, X. Tu and T. Shao, *Sustainable Energy Fuels*, 2022, **6**, 98–109.

170 G. Lee, D. B. Go and C. P. O'Brien, *ACS Appl. Mater. Interfaces*, 2021, **13**, 56242–56253.

171 E. C. Neyts, *Front. Chem. Sci. Eng.*, 2018, **12**, 145–154.

172 H.-H. Kim, Y. Teramoto, A. Ogata, H. Takagi and T. Nanba, *Plasma Chem. Plasma Process.*, 2016, **36**, 45–72.

173 S. Heijkers, M. Aghaei and A. Bogaerts, *J. Phys. Chem. C*, 2020, **124**, 7016–7030.

174 P. A. Maitre, M. S. Bieniek and P. N. Kechagiopoulos, *Chem. Eng. Sci.*, 2021, **234**, 116399.

175 P. Hongmanorom, J. Ashok, P. Chirawatkul and S. Kawi, *Appl. Catal., B*, 2021, **297**, 120454.

176 P. Hongmanorom, J. Ashok, G. Zhang, Z. Bian, M. H. Wai, Y. Zeng, S. Xi, A. Borgna and S. Kawi, *Appl. Catal., B*, 2021, **282**, 119564.

177 J. Ashok, M. L. Ang and S. Kawi, *Catal. Today*, 2017, **281**, 304–311.

178 S. Zhang, Y. Li, A. Knoll and G. S. Oehrlein, *J. Phys. D: Appl. Phys.*, 2020, **53**, 215201.

179 S. Xu, S. Chansai, S. Xu, C. E. Stere, Y. Jiao, S. Yang, C. Hardacre and X. Fan, *ACS Catal.*, 2020, **10**, 12828–12840.

180 Y. Sun, J. Wu, Y. Wang, J. Li, N. Wang, J. Harding, S. Mo, L. Chen, P. Chen, M. Fu, D. Ye, J. Huang and X. Tu, *J. Am. Chem. Soc.*, 2022, **2**, 1800–1810.

181 F. Hu, R. Ye, C. Jin, D. Liu, X. Chen, C. Li, K. H. Lim, G. Song, T. Wang, G. Feng, R. Zhang and S. Kawi, *Appl. Catal., B*, 2022, **317**, 121715.

182 S. Dell'Orco, N. Leick, J. L. Alleman, S. E. Habas and C. Mukarakate, *EES Catal.*, 2024, **2**, 1059–1071.

183 S. Zhang and G. Oehrlein, *J. Phys. D: Appl. Phys.*, 2021, **54**, 213001.

184 T. Suttikul, S. Nuchdang, D. Rattanaphra, T. Photsathain and C. Phalakornkule, *Int. J. Hydrogen Energy*, 2022, **47**, 30830–30842.

185 L. Liu, Z. Zhang, S. Das and S. Kawi, *Appl. Catal., B*, 2019, **250**, 250–272.

186 L. Liu, S. Das, T. Chen, N. Dewangan, J. Ashok, S. Xi, A. Borgna, Z. Li and S. Kawi, *Appl. Catal., B*, 2020, **265**, 118573.

187 K. Van Laer and A. Bogaerts, *Plasma Sources Sci. Technol.*, 2017, **26**, 085007.

188 S. Jo, T. Kim, D. H. Lee, W. S. Kang and Y.-H. Song, *Plasma Chem. Plasma Process.*, 2014, **34**, 175–186.

189 M. Młotek, J. Sentek, K. Krawczyk and K. Schmidt-Szałowski, *Appl. Catal., A*, 2009, **366**, 232–241.

190 K. Schmidt-Szałowski, K. Krawczyk and M. Młotek, *Plasma Processes Polym.*, 2007, **4**, 728–736.

191 T. Nozaki, A. Hattori and K. Okazaki, *Catal. Today*, 2004, **98**, 607–616.

192 J. Kim, J. Jeoung, J. Jeon, J. Kim, Y. S. Mok and K.-S. Ha, *Chem. Eng. J.*, 2019, **377**, 119896.

193 N. García-Moncada, G. van Rooij, T. Cents and L. Lefferts, *Catal. Today*, 2021, **369**, 210–220.

194 T. Mizushima, K. Matsumoto, J. Sugoh, H. Ohkita and N. Kakuta, *Appl. Catal., A*, 2004, **265**, 53–59.

195 T. Mizushima, K. Matsumoto, H. Ohkita and N. Kakuta, *Plasma Chem. Plasma Process.*, 2006, **27**, 1–11.

196 L. R. Winter, B. Ashford, J. Hong, A. B. Murphy and J. G. Chen, *ACS Catal.*, 2020, **10**, 14763–14774.

197 X. Gao, S. Deng and S. Kawi, *iScience*, 2022, **25**, 105343.

198 J. Xu, K.-G. Haw, Z. Li, S. Pati, Z. Wang and S. Kawi, *React. Chem. Eng.*, 2021, **6**, 52–66.

199 Z. Li, Y. Deng, N. Dewangan, J. Hu, Z. Wang, X. Tan, S. Liu and S. Kawi, *Chem. Eng. J.*, 2021, **420**, 129834.

200 T. Maneerung, K. Hidajat and S. Kawi, *J. Membr. Sci.*, 2016, **514**, 1–14.

201 Y. S. Lin and M. C. Duke, *Curr. Opin. Chem. Eng.*, 2013, **2**, 209–216.

202 S. Pati, S. Das, N. Dewangan, A. Jangam and S. Kawi, *Fuel*, 2023, **333**, 126433.

203 T. Maneerung, K. Hidajat and S. Kawi, *J. Membr. Sci.*, 2014, **452**, 127–142.

204 S. Pati, N. Dewangan, Z. Wang, A. Jangam and S. Kawi, *ACS Appl. Nano Mater.*, 2020, **3**, 6675–6683.

205 S. Pati, J. Ashok, N. Dewangan, T. Chen and S. Kawi, *J. Membr. Sci.*, 2020, **595**, 117496.

206 Y. Deng, Z. Li, T. Chen, Z. Bian, K. Lim, N. Dewangan, K. Giap Haw, Z. Wang and S. Kawi, *Chem. Eng. J.*, 2022, **435**, 133554.

207 Z. Li, Y. Deng, Z. Wang, J. Hu, K. G. Haw, G. Wang and S. Kawi, *J. Membr. Sci.*, 2021, **639**, 119682.

208 T. Chen, Z. Wang, L. Liu, S. Pati, M. H. Wai and S. Kawi, *Chem. Eng. J.*, 2020, **379**, 122182.

209 *United States Pat.*, 2021.